



RESEARCH ARTICLE OPEN ACCESS

Age-Dependent Finite Element Analysis of Microneedle Penetration into Human Skin: Influence of Insertion Velocity, and Microneedle's Geometry and Material

 Pouria Azarikhah^{1,2}  | Khaled Mohammed Saifullah^{1,2} | Zahra Faraji Rad^{2,3} 

¹School of Engineering, University of Southern Queensland, Toowoomba, Queensland, Australia | ²Centre for Future Materials, Institute for Advanced Engineering and Space Sciences, University of Southern Queensland, Toowoomba, Queensland, Australia | ³School of Science, Technology and Engineering, University of the Sunshine Coast, Petrie, Queensland, Australia

Correspondence: Zahra Faraji Rad (zahra.farajirad@unisq.edu.au; zfarajirad@usc.edu.au)

Received: 17 March 2025 | **Revised:** 30 June 2025

Funding: The authors received no specific funding for this work.

Keywords: finite element analysis | human age | insertion velocity | microneedle geometry | polymeric microneedle

ABSTRACT

Microneedles offer a minimally invasive alternative to hypodermic needles for drug delivery and point-of-care diagnostics. Previous studies on microneedle insertion force often used human skin with constant mechanical properties. However, this study, for the first time, investigates the combined effect of human age (29–68 years) and other variables such as insertion velocity (3 and 4.5 m/s), material (poly(glycolic acid) (PGA), Vectra MT-1300, and Zeonor 1060R) and geometry (cone-shaped and tapered cone-shaped) on insertion force using finite element analysis (FEA). The results show that insertion force increases significantly with age due to higher stratum corneum (SC) stiffness and failure criteria. For example, for a PGA cone-shaped microneedle at 4.5 m/s, the insertion force is 111.56%, 64.09%, 36.46%, and 10.52% higher for individuals aged 68, 53, 41, and 33 years, respectively, compared to 29 years. Microneedle material also significantly affects insertion force, with stiffer materials requiring less force to penetrate the SC. Cone-shaped microneedles exhibit lower insertion forces than tapered cone-shaped designs due to their smaller tip angle. Increasing insertion velocity substantially reduces the insertion force, with higher velocity having a more evident effect than changes in microneedle geometry. Finally, stress distribution within the microneedle and skin deformation are evaluated.

1 | Introduction

Different methods, such as oral, parenteral, inhalation, and transdermal routes, have been used to deliver medications into the human body for medical purposes. The oral route is the most convenient option for patients; however, in addition to poor absorption, prolonged use of medications may have unwanted side effects on body organs such as the liver, kidneys, and gastrointestinal tract [1]. Typical injection methods like conventional hypodermic needles present quick and direct drug delivery; however, it is often linked to needle anxiety, invasiveness, and

complications with venous access, such as fragile veins and difficulty in locating veins, which can hinder patient compliance, especially in vulnerable populations like infants and the elderly [2]. In addition to the required administration by trained personnel, hypodermic needles for vaccine delivery penetrate the muscle, where the immune response is weaker than in the skin [3, 4].

Transdermal drug delivery (TDD) systems, which allow for drug administration through the skin layers, are among the most effective and less invasive alternatives to traditional methods.

This is an open access article under the terms of the [Creative Commons Attribution](https://creativecommons.org/licenses/by/4.0/) License, which permits use, distribution and reproduction in any medium, provided the original work is properly cited.

© 2025 The Author(s). Macromolecular Materials and Engineering published by Wiley-VCH GmbH

Compared to other techniques, TDD offers a more controlled and sustained release of medication, minimizing the discomfort and risks associated with more invasive procedures [5, 6]. Microneedles, as a less invasive TDD system, provide a promising alternative that can enhance patient compliance and safety by reducing the pain and anxiety commonly associated with hypodermic needles. Drug delivery using microneedles is an innovative method that was initially introduced in 1976 [7]. These micron-sized needles pierce the skin's outermost layer, the SC, to form micro-channels to deliver drugs or vaccines into the epidermis or upper dermis with minimal invasiveness [8]. Microneedles present a versatile alternative to traditional hypodermic needles for a range of applications, including drug delivery, vaccinations, cosmetic procedures, and diagnostic testing [9, 10]. They provide benefits such as sustained drug release, reduced logistical costs, user-friendliness, easy disposal, and the potential to administer vaccines in remote areas [11].

Microneedles can be fabricated in various array configurations, shapes, and sizes, utilizing different materials and fabrication methods. In addition to the basic shapes of microneedles, such as pyramids, cylinders, and cones, various complex geometries, like tapered cones, bevelled tips, and octagonal cones, have been studied [12, 13]. Microneedles are generally 150–1500 μm in length, 50–250 μm in base width, and have a tip diameter ranging from 1–25 μm [8]. The aspect ratio of a microneedle is defined as the height to the base width or diameter, usually ranging from 2–10 for skin insertion [14]. Dimensional features like height, tip radius and angle, needle spacing, and the number of needles in an array are crucial for determining the mechanical strength and insertion efficiency of microneedles [15]. Microneedle tips are also made in various shapes, including cylindrical, triangular, pointed, pentagonal, and octagonal [16]. Reducing the tip radius of microneedles enhances insertion efficiency and lowers the force required to penetrate the SC [17]. Microneedles are classified into solid, hollow, coated, dissolving, and hydrogel-forming (HF) types, each tailored for specific medical applications.

Microneedles have been manufactured from silicon, metal, ceramic, non-degradable polymers, carbohydrates, and biodegradable polymers [18]. Even though silicon was the initial material used for microneedle fabrication, the fabrication cost is still high. Other challenges facing silicon microneedles are non-degradability, brittle nature, and the complicated multi-step manufacturing process involved in production [19, 20]. Metals provide several advantages, including outstanding mechanical properties, affordability, and biocompatibility. However, they are classified as non-degradable materials [21]. Ceramics exhibit high mechanical strength but are brittle under tensile loads [22].

In recent years, polymeric microneedles have been widely utilized to address challenges associated with manufacturing microneedles using other materials [23]. Polymeric materials are preferable due to their low cost, adequate mechanical strength, possible biocompatibility and biodegradability, and high chemical stability [21]. Biocompatible polymers are more affordable than other materials due to simpler fabrication processes and short processing cycles, which could help address microneedle scale-up production [24]. Moreover, polymeric materials can be used to manufacture almost all types of microneedles [25]. The non-toxicity of some biodegradable polymers allows various medical

solutions to be administered into the body using polymeric microneedles [26]. While polymers are less strong than metals, silicon, and ceramics, polymeric microneedles can still achieve sufficient mechanical properties for skin penetration by optimizing insertion factors such as insertion velocity and geometrical characteristics of microneedles like tip radius [27–30]. Various techniques have been employed to fabricate polymeric microneedles, including microinjection molding [31], hot embossing [32], casting [33], 3D printing [34], fused deposition modeling (FDM) [35], two-photon polymerization (TPP) [36], drawing lithography [37], and laser micromachining [38].

Human skin protects internal organs from biological, physical, and chemical harm. It behaves as an environmental regulator and serves as a medium for sensing stimuli, such as thermal and mechanical signals, through its receptors [39]. For effective TDD, microneedles must penetrate the SC, the skin's most compact layer in dry conditions [40, 41]. The SC, with an average thickness of 10–40 μm , is composed of elongated dead corneocytes enclosed by a lipid-rich matrix [42, 43]. To ensure the effective and safe insertion of microneedles into human skin, it is crucial to consider the mechanics of the skin and the microneedle, and the factors that affect penetration processes. The natural elasticity of the skin, along with the mechanical complexity of its layers, including the SC, viable epidermis, dermis, and hypodermis, influences the efficiency of microneedle insertion [44, 45]. During microneedle insertion, unforeseen excessive axial or lateral forces caused by the topology of the skin can lead to microneedle failure or breaking [46]. The mechanical properties of the SC make it the primary outer barrier against penetration of microneedles into the skin [47]. The dermis, typically 2–4 mm thick, lies beneath the dermo-epidermal junction and consists primarily of proteins, such as collagen and elastin, embedded in a mucopolysaccharide gel matrix. Collagen fibers provide the skin's tensile strength, while elastin enables the skin's elastic response to external forces [46]. The hypodermis, the deepest layer of the skin, functions as a heat insulator, provides mechanical support, and serves as a shock-absorbing cushion for underlying tissues [39].

Insufficient microneedle penetration through the SC results in low insertion efficiency, subsequently reducing the effectiveness of drug delivery or the extraction of interstitial fluid (ISF) for diagnostic purposes [48]. Penetration efficiency can also be affected by parameters like insertion velocity, shape, array density, material, medical application, and the size of the microneedles [49]. Optimizing geometrical and insertion parameters to reduce insertion force enhances the safety margin (SM), which is the ratio of microneedle failure force to microneedle penetration force [44, 50]. For instance, increasing microneedle spacing, decreasing tip area, and optimizing microneedle width and tip angle influence the insertion force [51]. Furthermore, applying vibration and increasing penetration speed using an applicator have been demonstrated to reduce the insertion force and improve penetration efficiency [50–53]. In addition to improving SM, reducing the penetration force will lead to a less invasive insertion [54].

FEA can effectively simulate microneedle insertion into human skin, offering a valuable alternative to complex experimental studies, often restricted by strict ethical regulations and experiment complexity. FEA models can calculate microneedle penetration efficiency and evaluate design modifications. Various

FEA studies have been conducted to investigate the factors influencing the penetration force of microneedles into multilayered human skin [55–58]. For example, Liu et al. [59] developed FEA to simulate the penetration of a cone-shaped microneedle into the skin, considering variables such as insertion velocity, tip area, tip angle, needle spacing, and skin thickness. Their results indicate that in order to reduce the insertion force effectively, the insertion velocity should be greater than 0.7 mm/s, the tip diameter should be less than 10 μm , and the needle spacing should exceed 200 μm . Wang et al. [60] demonstrated in their FEA study that microneedle spacing has a significant impact on insertion force. The findings indicated that increasing the spacing between microneedles results in a gradual reduction in penetration force; however, this effect becomes negligible beyond a spacing of 500 μm . The study identified 600 μm as the optimal spacing for microneedle arrays. Another FEA study by Zhang et al. [61] showed that the optimal spacing of hollow microneedle arrays depends on the microneedle material. Shu et al. [62] developed FEA models to study the insertion of solid stainless steel microneedles with a tip radius of 18 μm into hyperelastic, pre-stressed multilayered human skin. To account for the influence of neighboring microneedles on the overall response, they modeled the conical microneedles in an array. The findings indicated that increasing the skin's pre-tension from 0 to 10% strain resulted in a 13% reduction in penetration force. In another study, Ebrahiminejad et al. [51] conducted FEA to examine the insertion of a dissolving microneedle made from poly(vinyl alcohol) (PVA) and poly(vinylpyrrolidone) (PVP) polymeric materials into a multilayered hyperelastic skin model, considering skin stretch and microvibration effects. The FEA results showed a 32.31% decrease in insertion force at 10% strain and a 2.1% reduction at 150 Hz vibration. Kong et al. [63] conducted FEA by inserting a solid microneedle into multilayered human skin. The results indicated that the key factors influencing the insertion process include stiffness, failure stress, thickness of the SC, needle tip area, and wall angle. In contrast, other factors, such as the thicknesses of the dermis and hypodermis layers, had minimal impact. It was also observed that the force required to fracture microneedles increased with greater wall thickness, larger wall angle, and potentially a larger tip radius; the results were consistent with the FEA performed by Davis et al. [64]. Additionally, there is a linear relationship between the insertion force and the interfacial area of the microneedle tip [64]. Xenikakis et al. [65] developed an axisymmetric FEA model to study skin deformation, failure, and the insertion force involved in inserting a 3D-printed solid microneedle with a tip radius of 50 μm into human skin. The FEA results showed that the insertion force required to puncture the skin surface was 0.0308 N, equivalent to 1.1 N for 36 microneedles in an array.

In recent years, FEA has also been applied to assess the mechanical properties of polymeric microneedles, providing additional support to experimental results. The failure of microneedles poses risks, as residuals left in the body can lead to infection and further complications. To address these issues, improving the mechanical strength of microneedles through geometrical optimization and using biocompatible polymers with higher mechanical properties can increase safety. Takehara et al. [66] conducted an elastoplastic analysis using FEA on polymeric microneedles with high aspect ratios to determine optimal geometries that prevent elastoplastic deformation based on the mechanical properties of the poly-

mers. The study concluded that FEA provides essential design principles for microneedle geometries and creates guidelines for developing polymer microneedles and overcoming their mechanical weaknesses. Loizidou et al. [15] used FEA to evaluate the effects of different base shapes, such as triangular, square, and hexagonal, on the structural properties and skin penetration of microneedles. The findings showed a linear relationship between mechanical strength and the number of vertices in the polygonal base. The results indicate that microneedles can withstand higher compressive forces as the number of vertices increases. For example, hexagonal-based microneedles are less prone to fracture than those with a triangular base. Radhika and Gnanavel [67] performed FEA to evaluate the performance of polycarbonate (PC) and polyurethane (PU) tapered solid microneedles, each with a tip diameter of 60 μm , when inserted into human skin tissue. The study found that PC microneedles could endure the applied force of 40 N and avoid failure during insertion. Loizidou et al. [68] conducted experimental and FEA to examine the mechanical properties of sugar microneedles and assess how the sugar composition influences the ability of cone-shaped dissolving microneedles with a tip diameter of 10 μm to penetrate the skin and deliver drugs. The FEA results identified buckling as the primary cause of microneedle failure and demonstrated a correlation between Young's modulus of the sugar components, the predicted critical buckling load of the microneedles, and the depth of skin penetration. In another study, Kanakaraj et al. [69] simulated the penetration of a single microneedle with a tip diameter of 10 μm into human skin, considering various polymeric and non-polymeric materials for solid microneedles such as PC, polylactic acid (PLA), maltose, silicon, titanium, and silicon carbide. The analysis focused on factors influencing microneedle strength, such as buckling and bending forces. The results showed that silicon carbide outperformed the other materials. In contrast, PLA and PC were prone to buckling, making them less suitable among the materials tested.

Figure 1 comprehensively illustrates the parameters that influence the insertion force of microneedles into human skin, as reported in the literature. These factors include microneedles' features, such as mechanical properties and geometry, insertion procedures like velocity, and the properties of the skin itself. The mechanics of microneedle insertion and insertion force into human skin are crucial factors for the safe application of microneedles [70] but have received limited attention. Strict ethical regulations surrounding human testing make it difficult to experimentally study microneedle penetration in human skin across various age groups and skin models. This difficulty is compounded when other factors, such as insertion speed, microneedle material, and geometry, are modified. FEA offers an alternative, allowing predictions of microneedle insertion performance and enabling quick comparisons of design modifications, thereby reducing the reliance on expensive and time-consuming experiments when testing microneedles under various conditions [71].

Most prior studies have used a single model of human skin with constant mechanical properties and thicknesses for FEA. In these studies, the FEA of microneedle insertion into human skin was conducted without considering the variation of skin properties across different ages; therefore, a single skin property was applied to all cases [51, 56, 57, 59, 62, 65, 67, 73]. However,

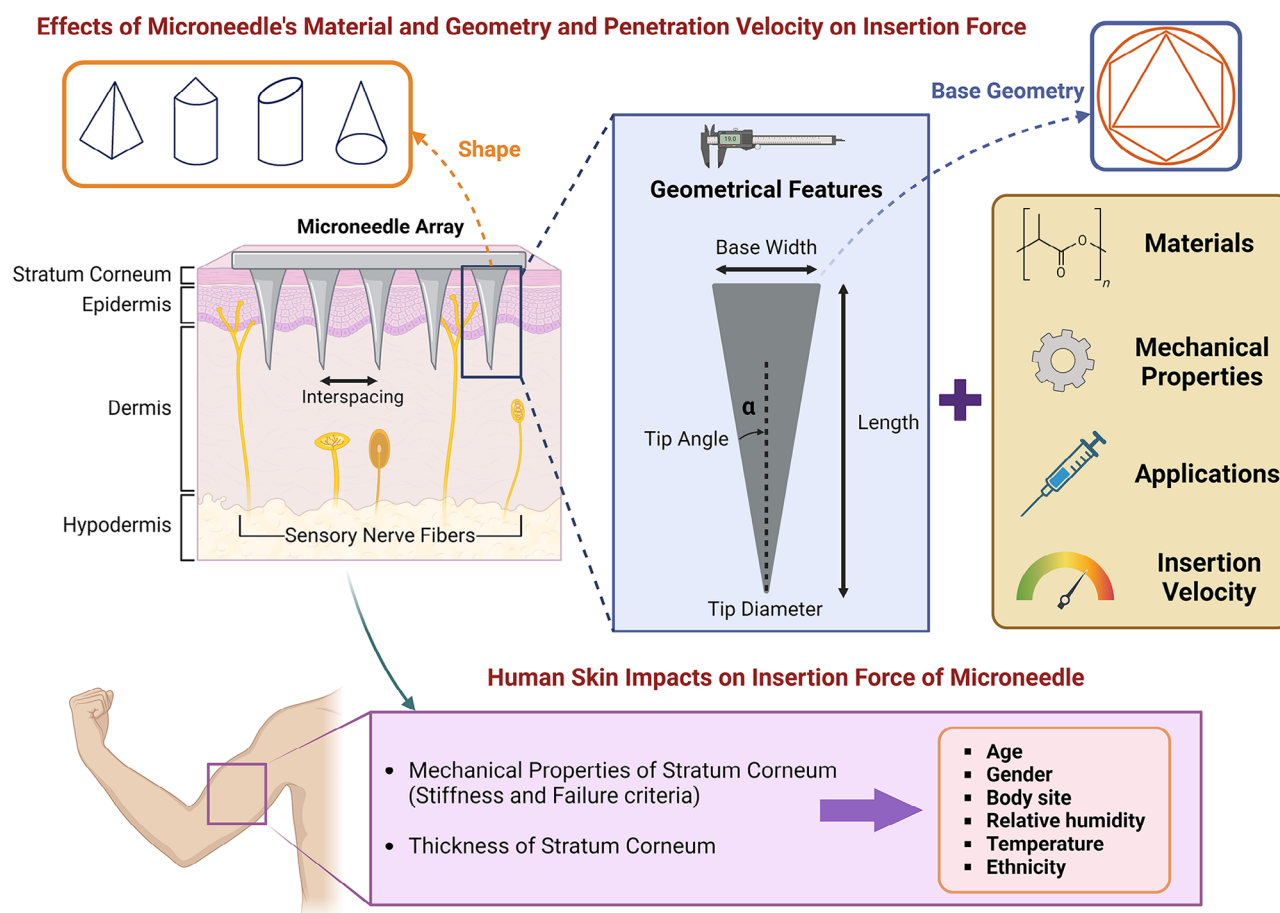


FIGURE 1 | A schematic representation of parameters affecting the insertion force of microneedles into human skin, as discussed in [44, 52, 64, 70, 72].

as the mechanical properties and thicknesses of the SC vary with age [74, 75], it is essential to examine microneedle insertion forces across different ages. Molak et al. [76] investigated the impact of human age on the mechanical properties of skin, showing that the highest Young's modulus values were observed in older donors. In a pilot study on the SC of Japanese women, Hara et al. [77] demonstrated that Young's modulus of the SC increased with age. In another age-related study, Biniek et al. [74] used micro-tension tests to demonstrate that the stiffness and fracture stress of the SC increase significantly with age.

For the first time, this study performs an age-dependent FEA to evaluate the force required for a microneedle to penetrate human skin, considering the various mechanical properties and thicknesses of the SC across different age groups. This topic has not been investigated in previous research but provides valuable information for customizing microneedle designs to suit the unique skin characteristics of patients at different ages [78]. Additionally, other variables, including insertion velocity and microneedle's material and geometry, were modified to simultaneously assess their impact on the insertion force across different age groups. This study exclusively examines two different microneedle geometries: (i) cone-shaped and (ii) tapered cone-shaped. For more precise data, a specific gender and body site was selected to minimize variation between specimens, allowing a more accurate comparison of results across

various human age groups. Moreover, according to the literature, most microneedle insertion studies were quasi-static, employing implicit models. In contrast, the current study employs explicit models, which are more suitable for short-duration events. The output of this comparative study will identify the trends and enable customizing microneedle designs per human age group.

2 | Materials and Methods

2.1 | Finite Element Models and Geometric Design of Microneedles

The FEA investigates the impacts of human age, the microneedle's material and geometry, and insertion velocity on the force required for a single microneedle to penetrate the SC of human skin. A series of geometric models were designed using ANSYS DesignModeler (2023 R1, ANSYS, Canonsburg, Pennsylvania, USA). The models included multilayered human skin with age-dependent SC thickness and a solid microneedle in two geometries: (i) cone-shaped and (ii) tapered cone-shaped. The microneedles featured a circular base diameter of 250 μm , a height of 1000 μm , a tip diameter of 3 μm , and an aspect ratio of 4:1. The tip angles of the cone-shaped and tapered cone-shaped microneedles are 7.04° and 26.29°, respectively.

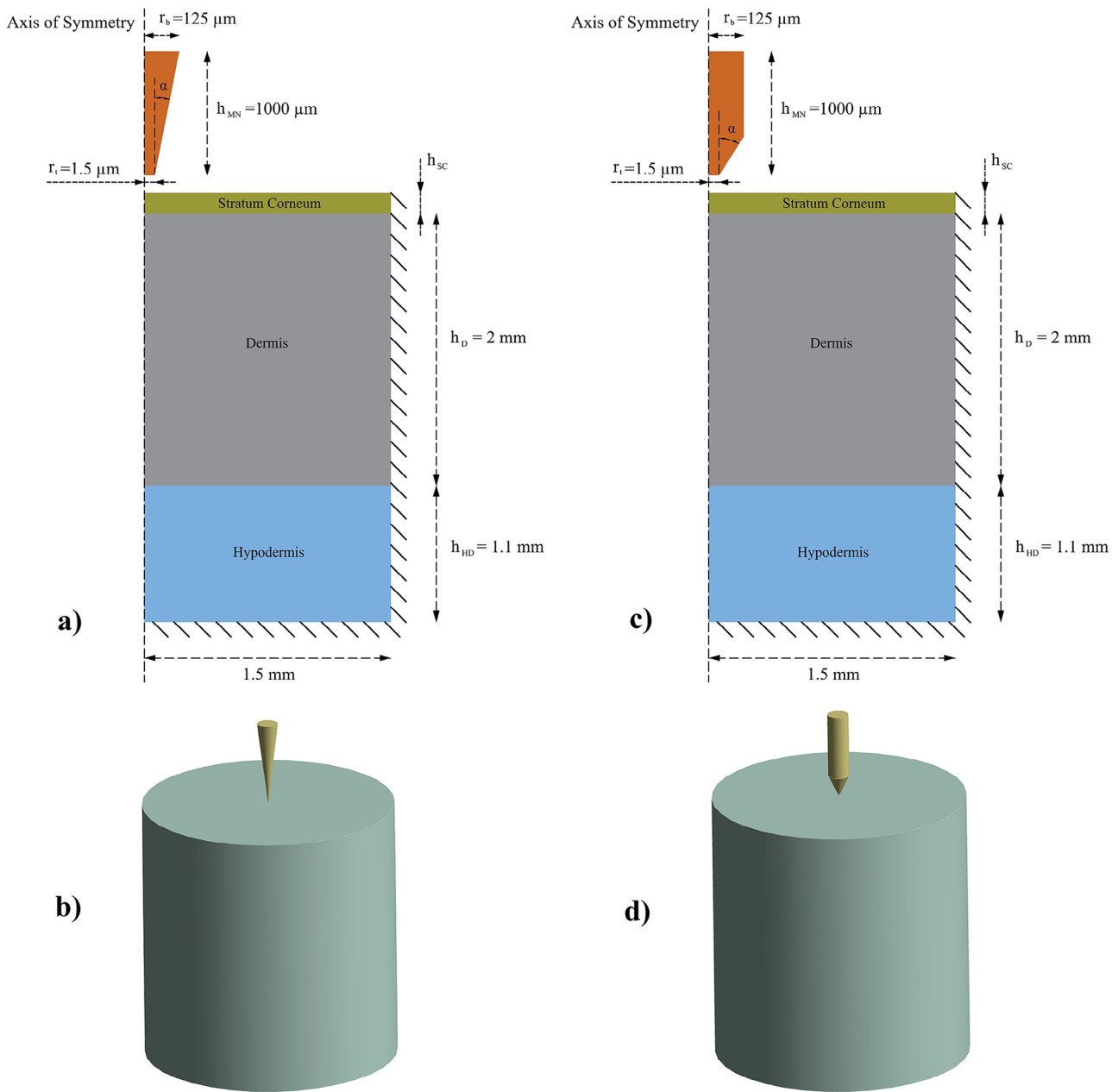


FIGURE 2 | (a) Dimensions and boundary conditions of the 2D axisymmetric model of the cone-shaped microneedle and multilayered human skin, (b) 3D model generated by revolving the 2D profiles of the cone-shaped microneedle and human skin around the axis of symmetry, (c) dimensions and boundary conditions of the 2D axisymmetric model of the tapered cone-shaped microneedle and multilayered human skin, (d) 3D model generated by revolving the 2D profiles of the tapered cone-shaped microneedle and human skin around the axis of symmetry.

FEA was conducted on a series of 2D axisymmetric models using the Explicit Dynamic module of ANSYS (2023 R1, ANSYS, Canonsburg, Pennsylvania, USA) to examine the insertion forces of solid microneedles with two distinct shapes (cone-shaped and tapered cone-shaped) into the SC of human skin. The study considered various ages (29, 33, 41, 53, and 68 years) and two impact velocities (3 and 4.5 m/s). The impact velocities were selected based on previous experimental studies involving the insertion of microneedles into porcine skin using custom-made applicators [51, 53, 73, 79]. The materials used for the microneedles include PGA, Vectra MT-1300, and Zeonor 1060R. Since there was no significant difference in insertion force between the 2D

axisymmetric and 3D models when considering isotropic material properties for the skin layers, the 2D axisymmetric models were used for all simulations to substantially reduce computational time while ensuring solution accuracy (Figure S1 and Table S1). The geometrical features and boundary conditions of the 2D axisymmetric models used in the FEA for the cone-shaped and tapered cone-shaped microneedles and the multilayered human skin are shown in Figure 2a,c, respectively. Furthermore, the 3D models were created by revolving the 2D surfaces of the cone-shaped and tapered cone-shaped microneedles and human skin around the axis of symmetry, as presented in Figure 2b,d, respectively.

TABLE 1 | Properties of microneedle materials used in ANSYS explicit dynamics.

Materials of microneedle	Density (kg/m ³)	Young's modulus (MPa)	Poisson ratio	Ultimate stress (MPa)	Refs.
Zeonor 1060R	1010	2100	0.49	53	[73, 80]
Vectra MT-1300	1400	7800	0.35	148	[81]
PGA	1530	9900	0.3	890	[82, 83]

TABLE 2 | Mechanical properties and thicknesses of SC across different human ages (abdominal samples from females at 7% relative humidity and 22°C).[51, 63, 74, 75]

Human age (years old)	Thickness (mean \pm SD) (μ m)	Young's modulus (MPa)	Poisson ratio	Density (kg/m ³)	Failure stress (MPa)
29	14.25 \pm 1.72	224.69	0.49	1300	20–44
33	15.10 \pm 1.58	245.68			
41	14.29 \pm 1.47	287.66			
53	14.00 \pm 1.90	350.63			
68	14.16 \pm 1.69	429.35			

The skin layers were composed of linear quadrilateral mesh elements, and specific bias types were applied to the edges of the layers to decrease the elements' size near the microneedle-skin interfaces, ensuring solution accuracy. A friction coefficient of 0.42 was used for the contact surfaces [62]. The contact formulation was defined using the penalty method. Furthermore, the microneedle tip surface was assigned as the contact surface, and the skin layers were considered the target surface. During insertion, the microneedle became surrounded by the skin layers. The erosion algorithm was implemented to facilitate the piercing of microneedles into the skin by eliminating mesh elements that reached their failure criteria while preserving their inertia effects. Additionally, fixed supports were applied to the lowest horizontal edge of the hypodermis and the farthest vertical edge of the entire skin model from the insertion point.

2.2 | Material Properties of Microneedles and Human Skin

Three biocompatible thermoplastic polymers, Zeonor 1060R, Vectra MT-1300, and poly(glycolic acid) (PGA), were used for microneedles. Table 1 presents the material properties used in the FEA study. These polymers were thermoplastic and selected as they are suitable for the mass production of microneedles using cost-effective techniques such as the microinjection molding technique [38].

The study assesses the insertion force required to pierce the skin. As the outermost and stiffest layer, the SC functions as a shield, protecting the underlying layers of the epidermis and presenting the main challenge for microneedle penetration. SC was part of the epidermis; since the other layers of the epidermis are significantly softer than the SC, and their exclusion had a negligible impact on the overall FEA results, only the thickness and stiffness of the SC were considered for modeling the epidermis [51, 57, 62,

63, 73]. Accordingly, the human skin model generated for FEA comprises three layers: the SC, the dermis, and the hypodermis.

The stiffness of the human SC was affected by age, along with other factors such as gender, body site, skin orientation, relative humidity, ethnicity, and temperature, all of which play a role in influencing the SC's mechanical behavior [44, 74]. In terms of gender, male skin generally exhibits greater hydration, transepidermal water loss, pigmentation, and thickness than female skin, resulting in differences in skin mechanics between genders [84]. These findings were supported by mechanical tests conducted by Serrat et al. [85] on the dorsal skin of male and female mice. In all cases, male skin demonstrated a higher elastic modulus and fracture toughness than female skin. Additionally, skin elastic recovery was significantly influenced by ageing, with the mechanical properties of male and female skin changing differently throughout life [86].

Regarding the anatomical site, Diridollou et al. [87] demonstrated that the skin on the forehead was thicker and had a higher Young's modulus than the forearm. These variations may be attributed to differences in the SC, epidermis, and dermis structure. Moreover, the forehead was more frequently exposed to sunlight than the ventral forearm, which may also contribute to the observed differences.

In this study, abdominal SC samples were selected from females aged 29, 33, 41, 53, and 68 at 7% relative humidity and 22°C to minimize variations between specimens under controlled conditions [74]. The selection of a specific gender and anatomical site aimed to ensure consistency and reduce the influence of biological variability. The dermis was modeled as a hyperelastic skin layer, using first-order Ogden material properties based on uniaxial test data [73, 88]. In contrast, the SC and hypodermis were assumed to exhibit linear elastic behavior. The FEA employs isotropic material models for each skin layer, which are either elastic or hyperelastic. Nevertheless, the whole skin is non-

TABLE 3 | Material properties and thicknesses of human skin's dermis and hypodermis.[62, 73]

Skin layer	Material model	Elasticity (MPa)	Poisson ratio	Hyperelastic coefficients	Incompressibility factor (MPa ⁻¹)	Density (kg/m ³)	Failure stress (MPa)	Thickness (mm)
Dermis	Ogden first order (Hyperelastic)	–	0.49	MU1: 0.0568 MPa, A1: 13.3	0.0745	1200	7	2
Hypodermis	Linear elastic	0.1	0.48	–	–	971	–	1.1

uniform due to its multilayered composition. Table 2 summarizes the material properties and thicknesses of SC across different human ages, and Table 3 summarizes the material properties and thicknesses of the human skin dermis and hypodermis considered in the study. The thickness of the SC was considered to vary with age, while the dermis and hypodermis were assigned constant thicknesses of 2 and 1.1 mm, respectively, due to their lower impact on FEA results [51]. In this study, the insertion force was defined as the force required to puncture the skin's primary barrier, the SC, which was stiffer than the dermis and hypodermis [57, 77]. Kong et al. [63] concluded that the thicknesses of the dermis and hypodermis had a negligible effect on microneedle insertion force. The results showed that increasing the thickness of the dermis and hypodermis leads to only a minimal change in the insertion force. Hara et al. [77] found no significant correlation between dermal Young's modulus and age. However, Alexander and Cook [89] reported that collagen in the dermis becomes stiffer with increasing age. Generally, it was well established that ageing leads to increased disorganization of collagen fibers and overall dermal degradation. This indicates that while age-related changes may have minimal impact on the elastic deformation of the dermis, they could substantially affect other mechanical characteristics, such as viscosity and elastic recovery [90, 91].

2.3 | Fundamental Theory of Insertion Force

The total insertion force of a single microneedle to pierce the skin's SC includes friction force, stiffness force, and cutting force, as described in Equation (1) [92].

$$F_{\text{insertion}} = F_{\text{stiffness}} + F_{\text{friction}} + F_{\text{cutting}} \quad (1)$$

When the microneedle tip contacts the skin surface, it compresses the SC. The force applied by the microneedle tip deforms the skin, eventually causing it to pierce. This displacement occurs before the bonds between the skin fibers break, allowing the microneedle to penetrate the skin [52]. The stiffness force arises before the SC is punctured and is determined by the skin's resistance to deformation due to its stiffness. This resistance causes the force to increase as the microneedle advances toward the skin. The friction force arises from the interaction between the contact surfaces of the microneedle and the skin during insertion. As the pre-rupture indentation force was applied to the skin, additional force was needed to cut through the skin, which depends on the microneedle's sharpness and the mechanical properties of the SC [62, 93]. The cutting force can be defined as the bond energy that holds the SC structure together. To

penetrate the SC, this energy must be overcome [52]. As shown in Equation (2), the total insertion force can be calculated using the work-energy principle, which states that the work done by the microneedle equals its change in kinetic energy from the initial impact velocity to the point of SC rupture.

$$w = \int_{x_1}^{x_2} F \cdot dx = F \cdot \Delta x = \Delta K = K_2 - K_1 \quad (2)$$

where F is the insertion force required for the microneedle to rupture the SC, Δx is the displacement of the microneedle until the SC is ruptured, and K_1 and K_2 represent the microneedle's initial kinetic energy and the kinetic energy at the point of SC rupture, respectively. In this study, the initial kinetic energy corresponds to two distinct impact velocities of 3 and 4.5 m/s. As the microneedle interacts with the SC, its velocity and kinetic energy decrease due to resistance from skin stiffness, friction, and cutting forces until the microneedle punctures the SC.

3 | Results and Discussion

The primary objective of this age-dependent FEA investigation is to evaluate the combined effects of human age, microneedle's material and geometry, and insertion speed on the force required to penetrate the SC for microneedle insertion, specifically focusing on human age. As the SC layer of skin serves as the primary barrier to microneedle penetration, the explicit dynamic simulation of microneedle insertion into human skin is focused on piercing the SC. FEA models evaluated the insertion forces required for penetrating a solid microneedle with two various geometries (cone-shaped and tapered cone-shaped) at five different ages (29, 33, 41, 53, and 68 years old) and two distinct impact velocities (3 and 4.5 m/s). The microneedles' materials are three thermoplastic polymers: PGA, Vectra MT-1300, and Zeonor 1060R.

Furthermore, the equivalent Von-Mises stress on the single microneedle during the penetration process and skin deformation are analyzed, considering all variables, including human age, insertion velocity, and the microneedle's geometry and material. Evaluating equivalent Von-Mises stress enables assessing the stress distribution in microneedles with varying geometries and materials during insertion across five different ages.

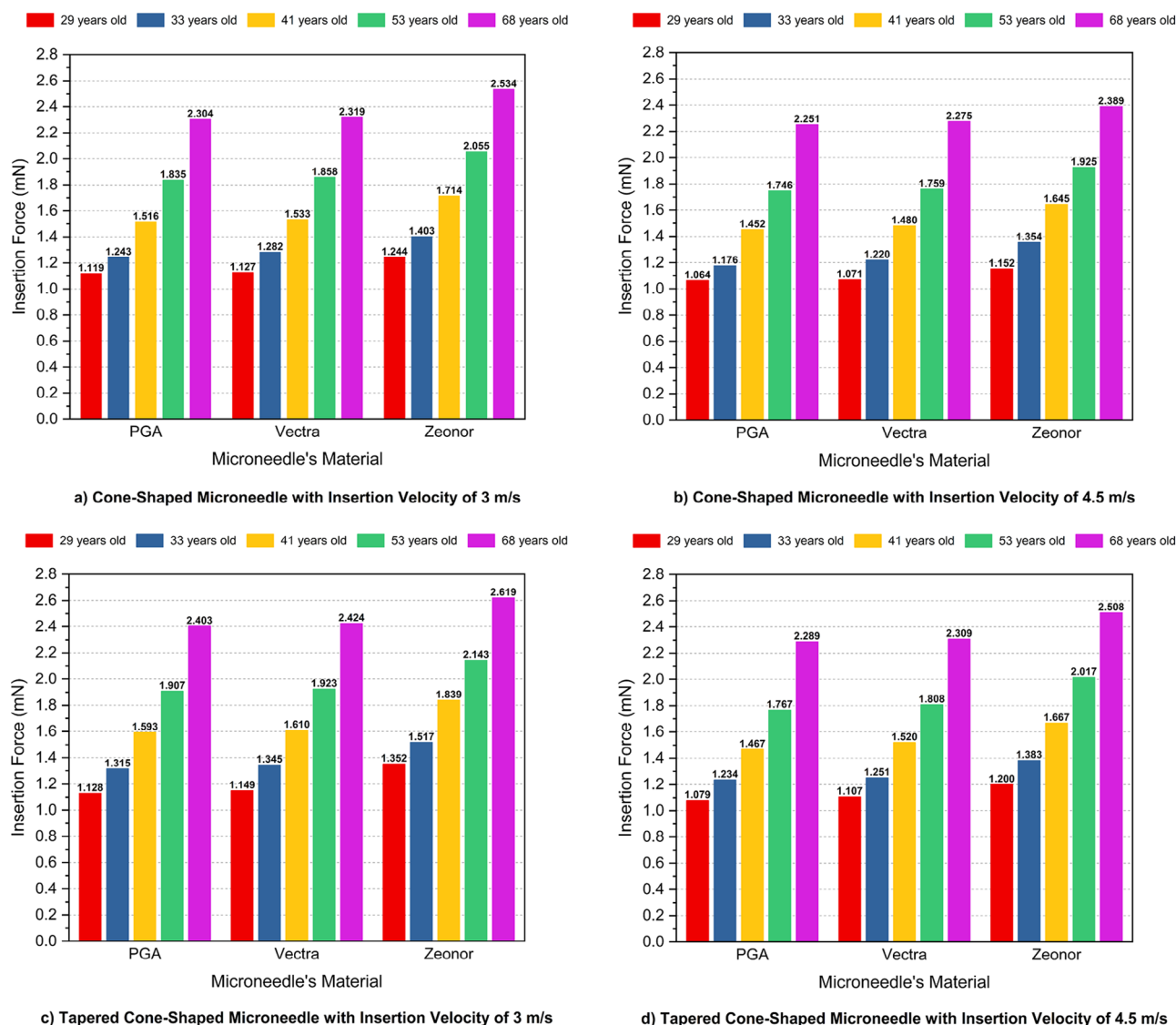


FIGURE 3 | Comparison of insertion forces for a single microneedle made from PGA, Vectra, and Zeonor materials into the SC of human skin across various ages (29, 33, 41, 53, and 68 years old), considering different microneedle geometries and insertion velocities, (a) cone-shaped microneedle with an insertion velocity of 3 m/s, (b) cone-shaped microneedle with an insertion velocity of 4.5 m/s, (c) tapered cone-shaped microneedle with an insertion velocity of 3 m/s, (d) tapered cone-shaped microneedle with an insertion velocity of 4.5 m/s.

3.1 | Insertion Force

3.1.1 | Combined Effects of Human Age and Microneedle Material on Insertion Force

The effects of human age and microneedle material on the insertion force required for a single microneedle penetrating the SC of different-aged human skins, considering various microneedle geometries and insertion velocities, are studied. The data presented in Figure 3 shows four bar charts, each representing a specific combination of microneedle geometry and insertion velocity. These include: (a) cone-shaped microneedle with an insertion velocity of 3 m/s, (b) cone-shaped microneedle with an insertion velocity of 4.5 m/s, (c) tapered cone-shaped microneedle with an insertion velocity of 3 m/s, and (d) tapered cone-shaped microneedle with an insertion velocity of 4.5 m/s. Each chart details the penetration force for three thermoplastic polymers, including PGA, Vectra MT-1300, and Zeonor

1060R, across five different human ages (29, 33, 41, 53, and 68 years).

The findings of this study demonstrate that for a tip radius of 1.5 μm , the insertion force ranges from 1.064 to 2.619 mN under all conditions. The results also show that the force of insertion to pierce the SC of human skin varies significantly with age. In all cases, the insertion force increased as the skin deformed, reaching a peak when the SC was pierced at the insertion point. After the puncture, the insertion force decreased (Figure S2). The mechanical properties of skin, particularly the SC, vary based on factors such as human age, hydration levels, body location, and individual differences. For instance, the failure stress of the SC tends to increase with age and decrease in relative humidity [63]. In this work, SC samples were obtained from the abdomens of females, and the data were collected under consistent conditions of 7% relative humidity and 22°C temperature to minimize variations between specimens. As shown in Figure 3, in all cases,

the insertion force increases with human age, which is attributed to the greater stiffness and higher failure criteria of the SC in older individuals. The findings align well with the previously reported study by Kong et al. [63], which used a series of 2D axisymmetric models of microneedle insertion into human skin with varying failure stresses. The study showed that increasing the failure criteria of SC leads to a higher insertion force.

It is concluded that the impact of SC thickness across different human ages is negligible, as their mean values are very similar and range from 14 to 15.10 μm . This finding aligns with a study by Kong et al. [63], which concluded that increasing the SC thickness from 10 to 30 μm results in only a 9.2% increase in microneedle insertion force. Under all conditions with similar microneedle geometries and insertion velocities, the maximum insertion force corresponds to the age group of 68 years. The other age groups, including 53, 41, 33, and 29, are placed in the next positions. The results emphasize the importance of considering age-related variations in skin properties when designing microneedles for specific applications. For instance, a cone-shaped microneedle made of PGA with an impact velocity of 4.5 m/s requires insertion forces that are 111.56%, 64.09%, 36.46%, and 10.52% higher to penetrate the SC of individuals aged 68, 53, 41, and 33 years, respectively, compared to a 29-year-old's SC. For a tapered cone-shaped microneedle made of Zeonor 1060R at an impact velocity of 3 m/s, the insertion forces needed to penetrate the SC of individuals aged 68, 53, 41, and 33 years are 93.71%, 58.5%, 36.02%, and 12.2% higher, respectively, than that required for a 29 years old SC.

For each specific microneedle geometry and insertion speed, the insertion forces varied significantly among the three polymers, highlighting the influence of microneedle material. Among the materials studied, PGA demonstrated the lowest penetration forces, while Zeonor 1060R consistently required the highest. This trend exhibits the impact of material stiffness on the microneedle's interaction with the SC. The greater the stiffness of the microneedle material, the lower the force required to puncture the SC. Stiffer microneedles undergo less deformation during insertion. This phenomenon allows for a more direct and efficient transfer of the insertion force to the skin, minimizing energy losses. Stiffer microneedle materials are more effective at localizing and directing stress at the microneedle's tip during insertion. The focused stress generates a high force concentration at the point of contact with the SC, which is critical for efficiently penetrating the skin surface.

In contrast, softer materials are more prone to deformation or slight blunting under insertion forces, reducing the tip's effectiveness. This increases contact resistance and requires greater force to pierce the SC successfully. For instance, using PGA as the microneedle material, the insertion forces are reduced by up to 13.06% for a cone-shaped microneedle at an insertion velocity of 3 m/s, 15.13% for a cone-shaped microneedle at 4.5 m/s, 19.85% for a tapered cone-shaped microneedle at 3 m/s, and 14.14% for a tapered cone-shaped microneedle at 4.5 m/s, compared to the softer Zeonor 1060R material across all individual human ages.

Considering the effects of human age and the microneedle's material for each specific microneedle geometry and insertion speed, the results indicate that the minimum insertion force occurs with

a microneedle made of PGA material when penetrating the SC of a 29-year-old human. In contrast, the maximum insertion force is observed with a microneedle made of Zeonor 1060R material when penetrating the SC of a 68-year-old human subject.

3.1.2 | Combined Effects of Human Age, Insertion Velocity, and Microneedle Geometry on Insertion Force

The combined effects of insertion velocity and microneedle geometry on the insertion force required to penetrate the SC are investigated across all studied human ages and microneedle materials. Figure 4a–c illustrates the insertion forces required for a solid microneedle to puncture the SC of human skin across ages ranging from 29 to 68. The data include two cone-shaped and tapered cone-shaped microneedle geometries and two penetration velocities of 3 and 4.5 m/s for PGA, Vectra MT-1300, and Zeonor 1060R microneedles.

The results show the dependencies of insertion force on all factors, including human age, microneedle geometry, and insertion velocity. As previously discussed, the findings demonstrate a consistent increase in insertion force with advancing human age, regardless of the penetration velocity and microneedle's material or geometry. This trend is attributed to the stiffening of the SC with age, which raises its resistance to penetration.

This study compares two microneedle geometries with a similar tip diameter of 3 μm : (i) a cone-shaped geometry and (ii) a tapered cone-shaped geometry, having tip angles of 7.04° and 26.29°, respectively. The results indicate that the cone-shaped microneedle consistently requires lower insertion forces across all conditions. The cone-shaped microneedle concentrates stress more effectively at the point of contact, facilitating easier insertion due to its smaller tip angle and sharper point. However, the tapered cone-shaped microneedle, with its larger tip angle, distributes force over a broader area, resulting in a higher required insertion force to penetrate the SC. These findings align with Ahn's [72] experimental results and demonstrate that the tip angle strongly influences the insertion force, highlighting the advantage of sharp-tip geometries in minimizing the force required for skin penetration. Furthermore, according to the experimental study by Jiang et al. [94] on the needle–tissue interaction forces, it was concluded that increasing the tip angle increases needle puncture force.

The insertion velocity plays a critical role in reducing the insertion force. Across all human ages and microneedle geometries, an impact velocity of 4.5 m/s results in lower insertion forces than 3 m/s. As defined in Equation (3), the force required to penetrate the SC of the skin surface shows a negative correlation with the microneedle's impact velocity. Higher velocity insertion of microneedles results in reduced insertion force, which aligns with the findings of Mahvash and Dupont's needle insertion model [95].

$$V_1 \langle V_2 \Rightarrow F(V_1) \rangle F(V_2) \quad (3)$$

Additionally, the results align with previously reported experimental findings using auxiliary insertion setups, such as applicators, by Ebrahiminejad and Faraji Rad [73], Ranamukhaarachchi

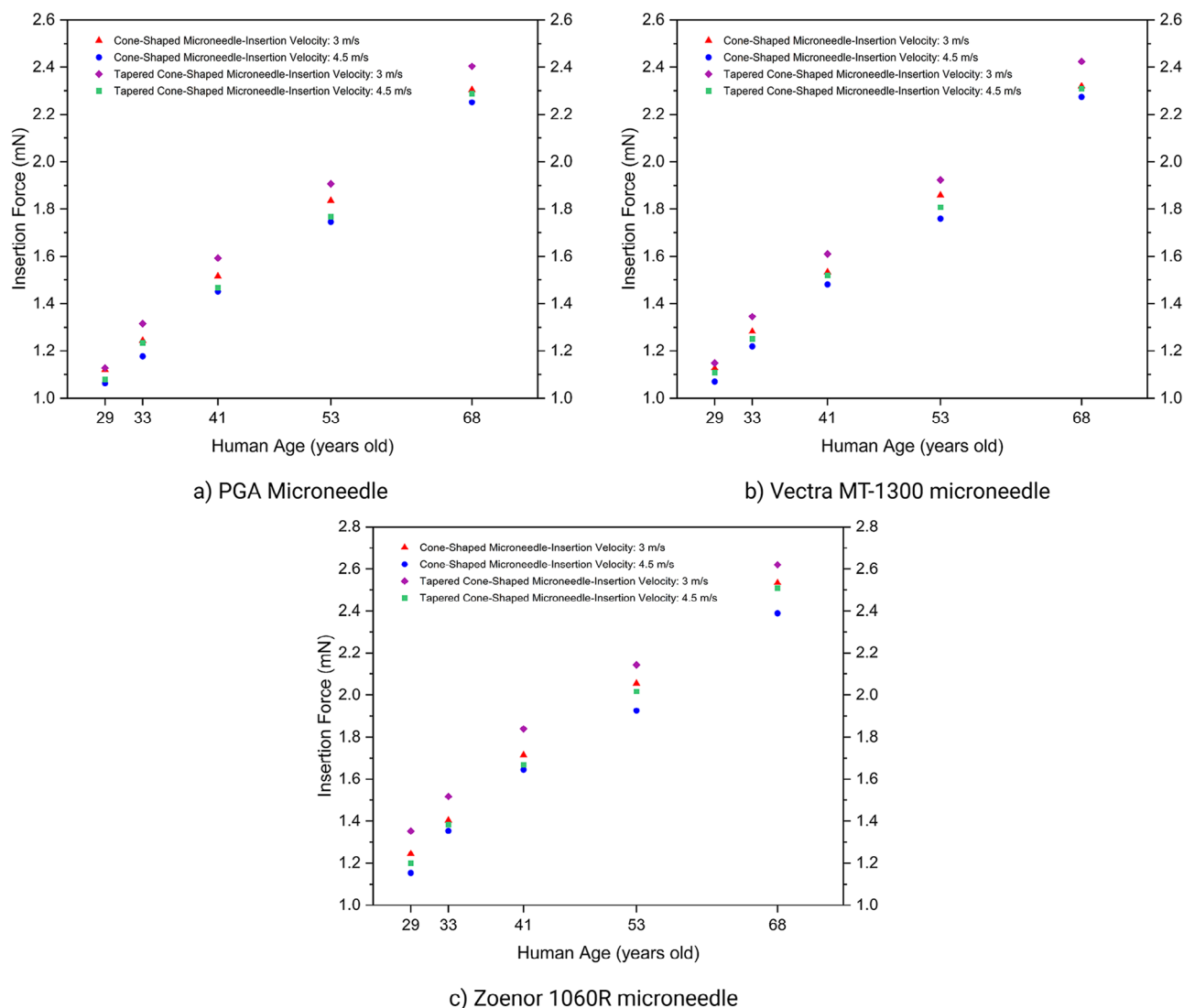


FIGURE 4 | Insertion forces for (a) PGA microneedle, (b) Vectra MT-1300 microneedle, and (c) Zenor 1060R microneedle, into the SC of humans aged 29, 33, 41, 53, and 68 years, considering cone-shaped and tapered cone-shaped microneedle geometry and insertion velocities of 3 and 4.5 m/s.

and Stoeber [50], and Olatunji et al. [52], which demonstrated that increasing the impact velocity of microneedles reduces the insertion force and improves the SM ratio. A possible reason for the decrease in insertion force with increasing impact velocity is the earlier development of localized stress concentrations in the SC of the skin model around the microneedle tip. This localized stress weakens the resistance of the SC, facilitating rupture and making the dynamic insertion process easier [50].

Figure 4a–c shows that the lowest insertion force corresponds to the cone-shaped microneedle at an insertion velocity of 4.5 m/s. Following this, the tapered cone-shaped microneedle at 4.5 m/s, the cone-shaped microneedle at 3 m/s, and the tapered cone-shaped microneedle at 3 m/s are placed in the following positions. These findings indicate that increasing the impact velocity from 3 to 4.5 m/s has a more pronounced effect on reducing the insertion force than altering the microneedle geometry from a tapered cone-shaped to a cone-shaped, which aims to decrease the tip angle. For example, for a 53-year-old individual using a Vectra microneedle, the SC rupture force for a cone-shaped microneedle

is 3.4% lower than that of a tapered cone-shaped microneedle at the same insertion velocity of 3 m/s. However, increasing the insertion velocity from 3 to 4.5 m/s for the tapered cone-shaped microneedle results in a 6.01% reduction in insertion force. When both the microneedle geometry is changed to cone-shaped and the insertion velocity is increased to 4.5 m/s, the insertion force decreases by 8.51% compared to the tapered cone-shaped microneedle at an impact velocity of 3 m/s.

3.1.3 | Combined Effects of Human Age, Microneedle Geometry, and Material on Insertion Force

This section demonstrates the combined effects of human age, microneedle geometry, and material on the insertion force required to penetrate the SC. The study assesses how variations in all conditions, including human ages (29, 33, 41, 53, and 68 years), microneedle geometry including cone-shaped (C) and tapered cone-shaped (T), and microneedle material (PGA, Vectra MT-1300, and Zenor 1060R), collectively influence the

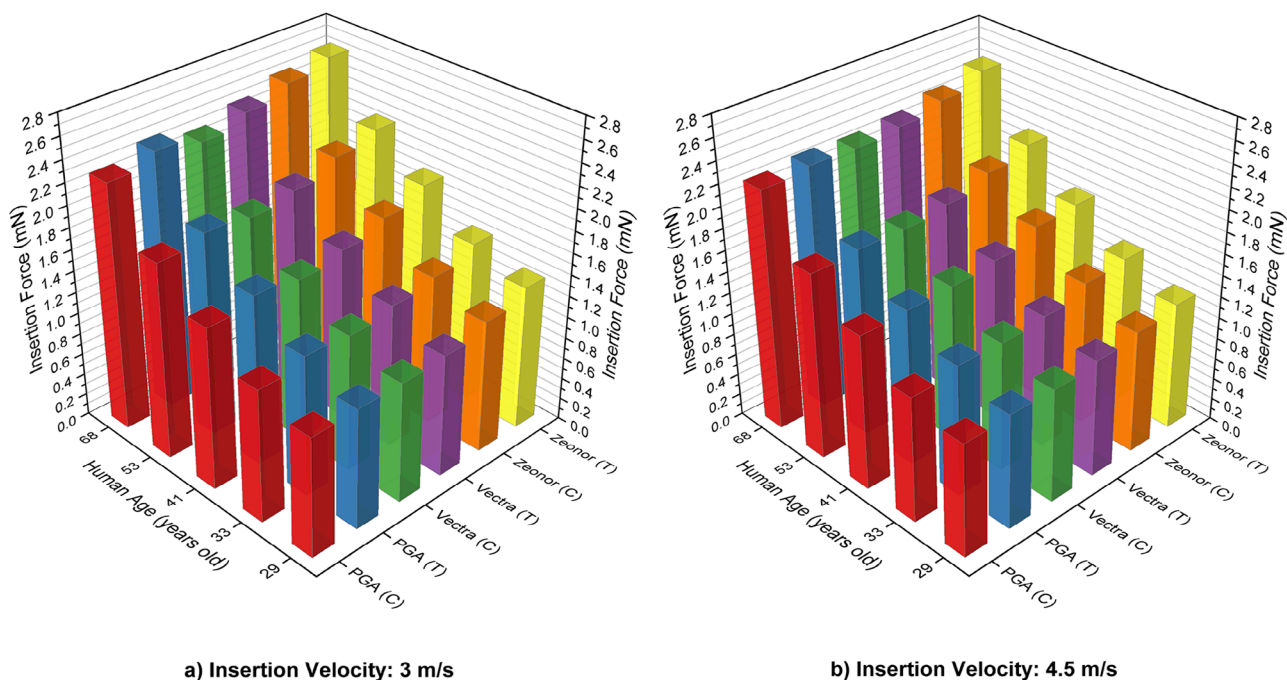


FIGURE 5 | Combined effects of human age (29, 33, 41, 53, and 68 years), microneedle geometry including cone-shaped (C) and tapered cone-shaped (T), and microneedle material (PGA, Vectra MT-1300, and Zeonor 1060R) on SC insertion force, with (a) insertion velocity of 3 m/s, and (b) insertion velocity of 4.5 m/s.

insertion force, independent of insertion velocity. The analysis provides a broader understanding of the interactive impact of all parameters on microneedle penetration into the SC. Figure 5 illustrates the insertion forces for microneedle penetration across various human age groups, combined with different microneedle materials and geometries, at two distinct insertion speeds: 3 and 4.5 m/s. The results indicate that the highest insertion force is associated with the Zeonor microneedle, which features a tapered cone-shaped geometry. Other microneedle structures, in descending order of insertion force, include Zeonor with a cone-shaped, Vectra with a tapered cone-shaped, PGA with a tapered cone-shaped, Vectra with a cone-shaped, and PGA with a cone-shaped. This trend remains consistent across all human age groups.

It is concluded that tapered cone-shaped microneedles require higher insertion forces than cone-shaped geometries, regardless of the material of the microneedle. However, in the case of Zeonor microneedles, their cone-shaped geometry still requires higher insertion forces than those of tapered cone-shaped microneedles made of PGA and Vectra. This irregularity can be attributed to the relatively low Young's modulus of Zeonor 1060R (2100 MPa) compared to Vectra MT-1300 (7800 MPa) and PGA (9900 MPa), which have values closer to each other. The lower stiffness of the Zeonor microneedle limits its ability to reduce insertion forces, even with a cone-shaped geometry. These findings underscore the critical influence of material properties and geometry of a microneedle on insertion force requirements, providing valuable insights for optimizing microneedle designs for various applications.

Apart from the general increase in insertion force with advancing age, the PGA microneedle with a cone-shaped geometry consistently exhibits the lowest insertion force across all age groups at

an impact velocity of 4.5 m/s. This is attributed to the combination of the highest stiffness of the PGA material, the smaller tip angle of the cone-shaped geometry, and the increased insertion velocity. Additionally, among the studied age groups, the lowest penetration force is observed in the SC of the youngest individual, aged 29 years.

3.1.4 | Reliability of Results Compared to Existing Experimental and FEA Data

Conducting experimental penetration tests of microneedles on human skin across various age groups and skin models is extremely challenging due to strict ethical regulations. The complexity increases further when considering additional variables such as insertion velocity, microneedle material, and geometry. While direct experimental validation of the microneedle insertion forces into human skin was not performed in this study, the results show similarities with previously reported values in the literature. Ling et al. [96] experimentally investigated the insertion force of an ultra-sharp worker honeybee stinger, used as a biomimetic microneedle, with a tip radius ranging from 1 to 1.5 μm , into artificial human skin. The study concluded that the penetration force ranged from 0.34 to 4.02 mN, with an average value of 1.34 mN. In this study, for a tip radius of 1.5 μm , the insertion force varies from 1.064 to 2.619 mN, which correlates well with the findings of Ling et al. [96].

Additionally, to verify the insertion force values obtained from this FEA study, the ratio of insertion force to microneedle tip area/radius is compared with previously reported numerical and experimental data. Generally, the force required for insertion is proportional to the tip area and, accordingly, to the tip radius of

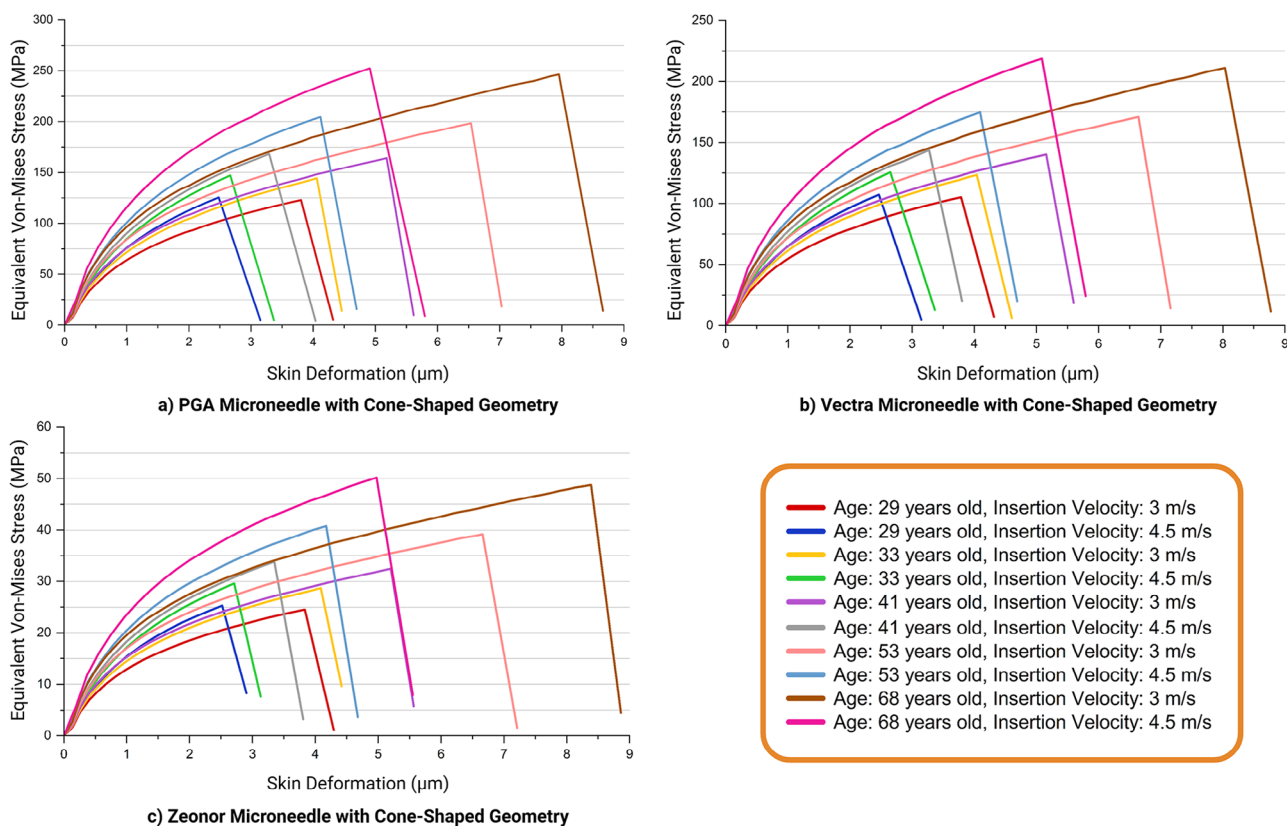


FIGURE 6 | The maximum equivalent Von-Mises stress applied to a cone-shaped microneedle during insertion into the SC of human skin is shown considering the skin deformation at different ages (29, 33, 41, 53, and 68 years) and insertion velocities of 3 and 4.5 m/s for (a) PGA microneedle, (b) Vectra MT-1300 microneedle, and (c) Zeonor 1060R microneedle.

the microneedle, which is consistent with a balance between the energy applied to the skin and the energy needed to create a tear inside the skin [97]. A linear relationship between the insertion force (F) of a microneedle and the tip area (A_{tip}) is expressed in Equation (4), where m is the ratio of microneedle insertion force to tip surface area [98].

$$F = m \times A_{tip} \quad (4)$$

The constant m depends on various factors, including the material properties of the microneedle, the mechanical properties of the skin, the tip angle, the insertion velocity, and other needle-skin interaction variables. Park et al. [98] experimentally measured the insertion force of microneedles fabricated of poly-L-lactic acid (L-PLA) into human skin. The best-fit linear regression of the results showed that the constant m in the study was $0.00012 \text{ N}/\mu\text{m}^2$. Furthermore, experimental measurements and theoretical modeling of the insertion of metal hollow microneedles into human subjects demonstrated that across a range of microneedle geometries, the insertion force into human skin depends strongly and linearly on the cross-sectional area of the needle tip [64]. The investigation showed that the constant m was $0.00019 \text{ N}/\mu\text{m}^2$. In this study, the constant m , is defined as the ratio of insertion force to tip surface area, ranging from 0.00015 to $0.00037 \text{ N}/\mu\text{m}^2$, which matches the values obtained in previous studies [64, 98].

The results also show a strong correlation with previous experimental and numerical studies in terms of the ratio of insertion force to tip radius. For example, Ling et al. [99] reported an

average penetration force of 5.75 mN for inserting a honeybee stinger as a biomimetic microneedle with a tip radius of $1.5 \mu\text{m}$ at an insertion velocity of 0.05 mm/s into rabbit skin. Similarly, Shu et al. [62] presented FEA results indicating a penetration force of 30.5 mN for a solid stainless steel microneedle with a tip radius of $18 \mu\text{m}$ at an insertion velocity of 0.3 mm/s . Olatunji et al. [52] experimentally demonstrated that the insertion force of a single microneedle made of poly(methyl vinyl ether and maleic anhydride) (PMVE-MA), with a tip radius of $30 \mu\text{m}$, ranges from 28 to 30 mN when inserted into human skin at a velocity of 0.5 mm/s . Another study [64] showed that the insertion force of a stainless steel microneedle with a $30 \mu\text{m}$ tip radius into human skin was 80 mN at an insertion velocity of 1.1 mm/s . Additionally, a study conducted by Zhang et al. [57] demonstrated that the insertion force of a PLA microneedle with a tip radius of $10 \mu\text{m}$ into multilayered human skin at a constant insertion velocity of 1 mm/s was 5.9 mN. Xenikakis et al. [65] reported inserting a solid polymer-based microneedle with a tip radius of $50 \mu\text{m}$ into human skin at a constant velocity of 0.5 mm/s ; a penetration force of 30.8 mN was required. In the abovementioned studies, the microneedle insertion force to tip radius ratios were 3.83 [99], 1.7 [62], ≈ 1 [52], 2.67 [64], 0.59 [57], and 0.616 [65] mN/ μm . The ratio of insertion force to microneedle tip radius in this study, for a microneedle with a tip radius of $1.5 \mu\text{m}$, ranges from 0.71 to 1.746 mN/ μm under all conditions, which aligns with reported data in the literature.

Overall, despite differences in microneedle materials, geometries, insertion speeds, and test subjects between this study and

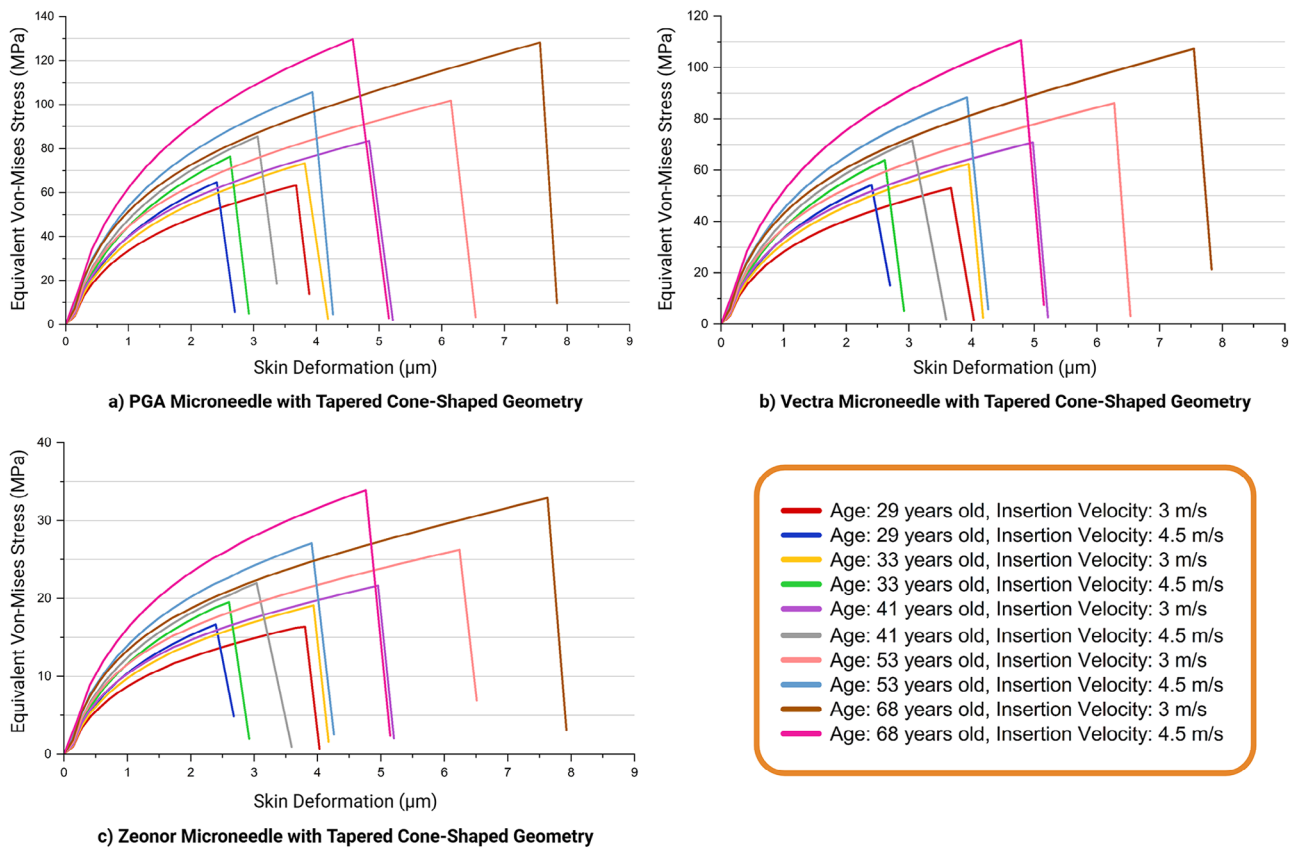


FIGURE 7 | The maximum equivalent Von-Mises stress applied to a tapered cone-shaped microneedle during insertion into the SC of human skin is shown considering the skin deformation at different ages (29, 33, 41, 53, and 68 years) and insertion velocities of 3 and 4.5 m/s for (a) PGA microneedle, (b) Vectra MT-1300 microneedle, and (c) Zeonor 1060R microneedle.

previous works [52, 57, 62, 64, 65, 98, 99], the results, when expressed as the ratio of insertion force to either microneedle tip area or tip radius, strongly correlate with previously reported models and experimental findings, reinforcing the reliability of data presented. Since no direct experimental validation based on human age is available for this study, an experimental setup for inserting polymeric microneedles into human skin of different ages is proposed for future considerations (Supporting Information, Section S3).

3.2 | Stress Distribution Within Microneedle and Skin Deformation During Insertion

The equivalent Von-Mises stress provides a scalar measure of the combined stress distribution within the microneedle during insertion into the SC of human skin (Videos S1 and S2). In this study, FEA is conducted using the Explicit Dynamic module of ANSYS (2023 R1, ANSYS, Canonsburg, Pennsylvania, USA) on 2D axisymmetric models to determine the equivalent Von-Mises stress in a solid microneedle. This allows for a comparison of the effects of parameters such as human age, microneedle geometry, microneedle material, and insertion velocity on the stress distribution in the microneedle during penetration into human skin.

Figures 6 and 7 illustrate the maximum equivalent Von-Mises stress of a single microneedle during insertion into the SC of

human skin, highlighting the deformation of the skin. Figure 6 represents cone-shaped microneedles, while Figure 7 shows tapered cone-shaped microneedles. Three different microneedle materials were evaluated for each geometry, including PGA, Vectra MT-1300, and Zeonor 1060R. The Figures for each material include data corresponding to different human ages (29, 33, 41, 53, and 68 years) and two penetration velocities of 3 and 4.5 m/s. In all cases, the equivalent Von-Mises stress increased as the skin deformed, reaching a peak when the SC pierced at the insertion point. After penetration, the stress decreased due to the resistance relief at the insertion site. The results show notable differences in equivalent Von-Mises stress and skin deformation patterns based on human age, microneedle material and geometry, and insertion velocity.

For both geometries and all materials, the skin deformation at the penetration point increased with human age. This trend is attributed to the increased stiffness and higher resistance of the SC in older individuals, which prolongs the deformation phase before insertion and requires greater deformation before failure. Increasing the insertion velocity from 3 to 4.5 m/s reduced skin deformation at the point of penetration. The higher velocity allowed the microneedle to rapidly overcome the SC's resistance, reducing the extent of skin deformation required for penetration.

The maximum equivalent Von-Mises stress increases with human age as the SC of older skin is stiffer, requiring higher forces to penetrate. This relationship highlights the need to tailor microneedle

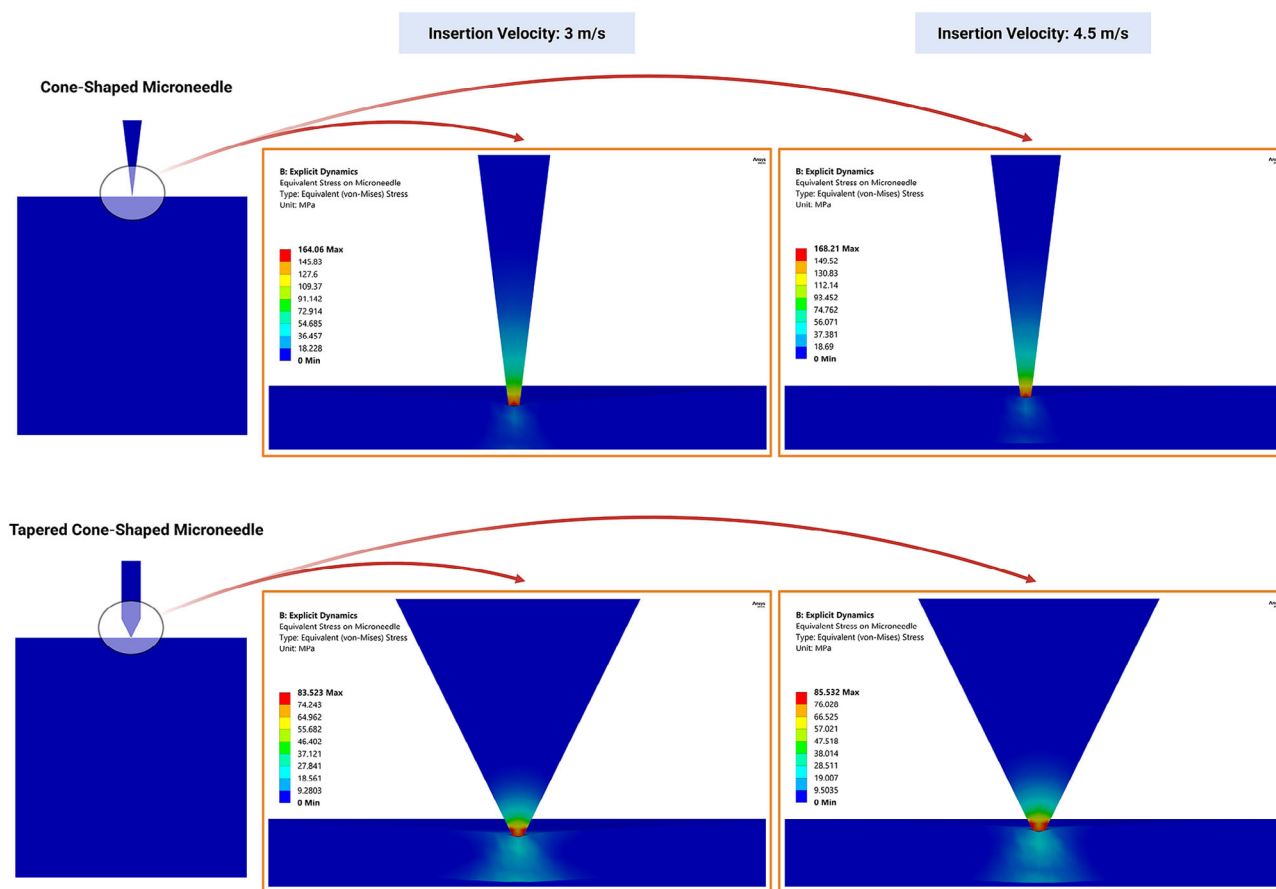


FIGURE 8 | A cross-sectional view of maximum equivalent Von-Mises stress on a cone-shaped and a tapered cone-shaped microneedle made of PGA material before penetration of the SC of 41-year-old human skin at insertion velocities of 3 and 4.5 m/s.

designs based on human age to prevent excessive stress on the microneedle, which might lead to needle failure during penetration. Cone-shaped microneedles consistently exhibited higher peak stresses compared to tapered cone-shaped designs. This is attributed to the lower tip angle and higher sharpness of the cone-shaped geometry, which leads to greater stress concentration at the microneedle's tip. A sharper tip on microneedles allows for easier skin penetration with minimal force. However, the increased sharpness also makes the microneedles more prone to excessive stress. This difference highlights the influence of geometry on stress distribution during microneedle insertion, demonstrating that tapered designs achieve a more favorable stress profile.

Among the three materials, PGA microneedles, with the highest Young's modulus, exhibited the highest maximum equivalent Von-Mises stress. Vectra MT-1300 and Zeonor 1060R materials are placed in the following positions. The FEA shows that a material like PGA, which has a higher Young's modulus, can experience higher stress than materials with lower stiffness such as Zeonor. According to Hooke's law, materials with higher stiffness resist deformation under applied loads and transmit forces more directly to the microneedle's tip, which serves as the contact point with the skin [55, 100]. Consequently, stiffer materials deform less and do not distribute stress as effectively as softer materials, leading to higher localized stresses in critical areas of the microneedle, such as the tip. As previously discussed, microneedles made from materials with higher Young's

modulus are more effective at localizing and directing stress to the microneedle's tip during insertion, resulting in a lower required insertion force. In contrast, softer materials can absorb and dissipate more energy through elastic deformation. Stiffer materials lack this energy absorption capacity, causing more stress to accumulate within the microneedle structure. Additionally, a stiffer microneedle imposes higher stress on the skin, further increasing the reaction stress applied to the microneedle. While higher insertion velocity slightly increases the maximum equivalent Von-Mises stress due to inertial effects, the impact is negligible compared to the influence of the microneedle's material properties and geometry.

Figure 8 presents the cross-sectional view of the FEA results from 2D axisymmetric models for equivalent Von-Mises stress on a cone-shaped and a tapered cone-shaped microneedle made of PGA prior to penetrating the SC of a 41-year-old human skin at insertion velocities of 3 and 4.5 m/s. The results enable a comparison of the effects of microneedle geometry and insertion velocity on the equivalent Von-Mises stress applied to the microneedles. Regions highlighted in red indicate the areas of highest stress, consistently observed at the microneedle tip across all cases. At an insertion velocity of 3 m/s, the maximum equivalent Von-Mises stress at the cone-shaped microneedle tip is 164.06 MPa, which decreases to 83.523 MPa for the tapered cone-shaped microneedle at the same velocity. This reduction demonstrates that increasing the tip angle lowers stress levels, thereby decreasing the likelihood of tip breakage. Although higher insertion velocities

Guidance for Microneedle Design Considering Age-Dependent Skin Properties

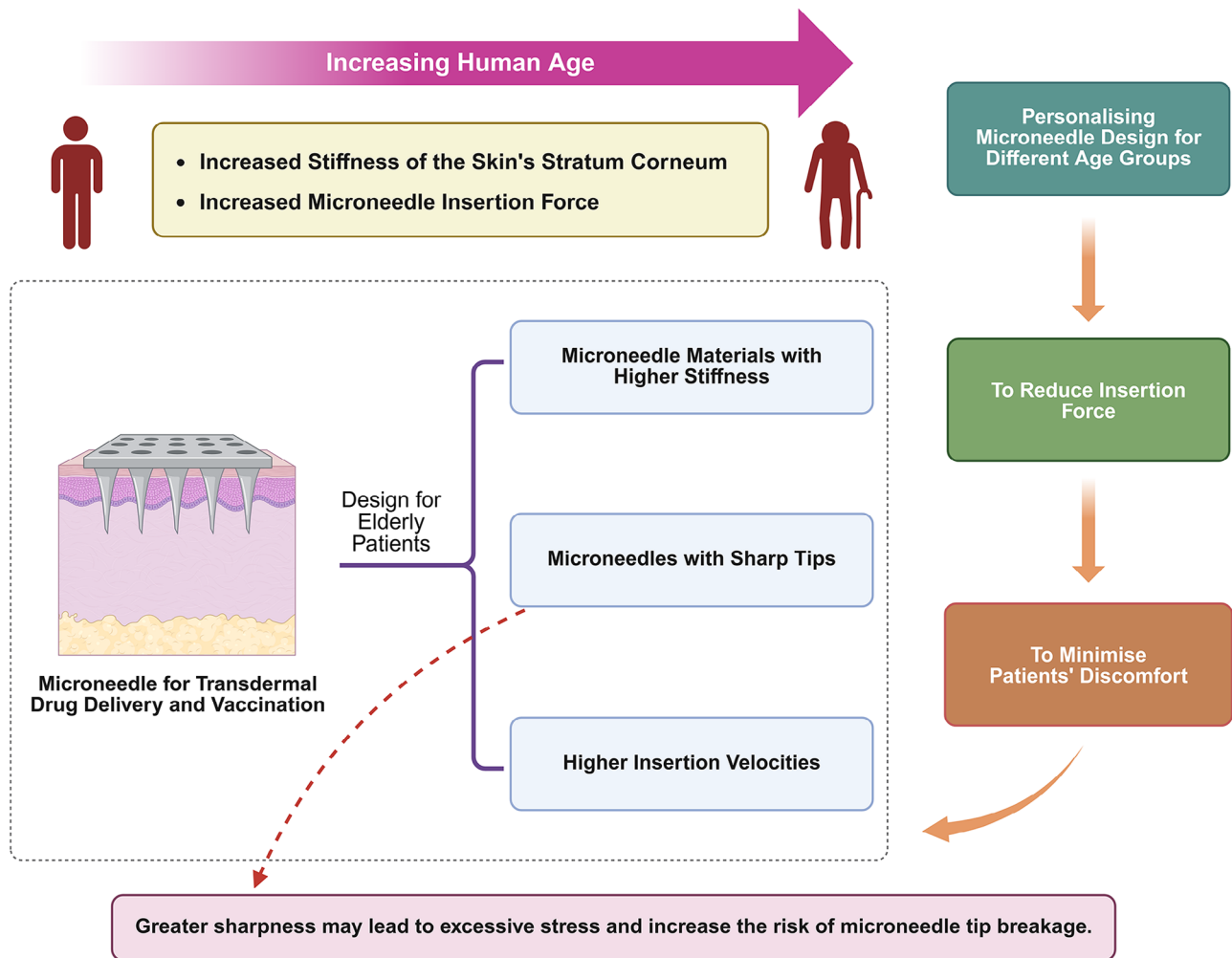


FIGURE 9 | Guidance for microneedle design based on age-related variations in skin properties, focusing on elderly individuals.

result in a slight increase in the maximum equivalent Von-Mises stress, their effect is minimal compared to the more substantial influence of microneedle geometry. However, increasing the insertion velocity reduces skin deformation before puncturing the human skin.

These findings emphasize the importance of optimizing microneedle design and material selection to ensure mechanical reliability across diverse application scenarios. The tapered cone-shaped design consistently exhibits lower Von-Mises stress than the cone-shaped design, making it a more robust and reliable choice for all tested conditions. Furthermore, materials with higher elasticities provide a greater safety margin and reduce the risk of failure, even in challenging scenarios involving older skin. In contrast, cone-shaped microneedles made of less elastic materials are more prone to high-stress concentrations, particularly for older patients.

4 | Conclusions and Future Perspectives

This study uses explicit dynamic FEA to present the first comprehensive analysis of the force required for micronee-

dles to penetrate the SC of human skin across different ages. By evaluating the combined effects of microneedle material, geometry, and insertion velocity, different scenarios are determined to guide the development of age-specific microneedle designs.

The study used multilayered human skin models derived from abdominal SC samples of females aged 29, 33, 41, 53, and 68 years, incorporating two insertion velocities (3 and 4.5 m/s) and three thermoplastic microneedle materials (PGA, Vectra MT-1300, and Zeonor 1060R) and two microneedle geometries (cone-shaped and tapered cone-shaped). The results indicated that the insertion force increased with age, with the highest force required for 68-year-old skin due to increased SC stiffness, followed by 53, 41, 33, and 29 years. PGA consistently required the lowest insertion force among materials due to its superior stiffness, while Zeonor 1060R needed the highest. The Young's modulus of the microneedle material proved to be a key factor in minimizing insertion force. Geometry also played a crucial role: cone-shaped microneedles required lower forces due to their sharper tips but were more prone to stress-induced breakage than tapered cone-shaped designs. Increasing insertion velocity from 3 to 4.5 m/s significantly reduced insertion forces, with a greater

impact than changes in geometry. The outcomes emphasize that increasing the velocity from 3 to 4.5 m/s has a more significant effect on reducing insertion force than modifying the geometry from a tapered cone-shaped to a cone-shaped. The optimal configuration across all age groups was a PGA microneedle with a cone-shaped geometry and an insertion velocity of 4.5 m/s, offering the lowest insertion forces. The reason is the combined impacts of the PGA material's high stiffness, the smaller tip angle of the cone-shaped geometry, and the higher insertion velocity. Conversely, with a tapered cone-shaped geometry, the Zeonor microneedle, at 3 m/s, was associated with the highest insertion force.

Cone-shaped microneedles exhibited significantly higher peak stresses than tapered cone-shaped designs, as their sharper tips lead to greater stress concentration, which increases the likelihood of tip breakage. While higher insertion velocities slightly raised stress levels, they significantly reduced pre-puncture skin deformation. The sharp tip of cone-shaped microneedles facilitates easier skin puncture with minimal required force. However, more sharpness also increase stress concentration at the tip, making microneedles more vulnerable to breakage and raising the risk of failure. Tapered cone-shaped microneedles demonstrated a more favorable stress distribution and consistently lower stress values, ensuring better performance across all studied conditions. Materials with higher stiffness, such as PGA, enhance safety margins, reducing the risk of failure, particularly for older skin.

In summary, this study highlights the critical importance of personalizing microneedle design, considering age-related variations in the SC of human skin. By evaluating the microneedle's material, geometry, and insertion velocity, this research offers valuable guidance for designing microneedles tailored to different age groups, particularly in applications such as transdermal drug delivery and vaccination. As insertion force increases with age due to higher SC stiffness, optimizing microneedle performance becomes critical to ensure reliable penetration and minimize patient discomfort. For elderly patients, selecting materials with higher stiffness, such as PGA, is essential to reduce insertion force and prevent microneedle structural failure. Additionally, using microneedles with lower tip angles, such as the cone-shaped design, and at higher insertion velocities (e.g., 4.5 m/s) can further enhance performance by reducing the required force, leading to a more efficient and less invasive insertion process. However, lower tip angles may also increase the risk of microneedle breakage, particularly in elderly patients, due to higher stress concentrations at the tip. Figure 9 illustrates how microneedle design is guided by age-related variations in human skin, with a specific focus on elderly patients, based on the findings of this study.

Acknowledgements

Open access publishing facilitated by University of the Sunshine Coast, as part of the Wiley - University of the Sunshine Coast agreement via the Council of Australian University Librarians.

Conflicts of Interest

The authors declare no conflict of interest.

Data Availability Statement

The data that support the findings of this study are available in the supplementary material of this article

References

1. Y. C. Kim, J. H. Park, and M. R. Prausnitz, "Microneedles for Drug and Vaccine Delivery," *Advanced Drug Delivery Reviews* 64 (2012): 1547–1568.
2. F. R. Zahra, N. Robert, D. Graham, A. C. John, and P. Philip, "Microfluidic Devices and Fabrication," *US 10850082 B2* (United States Patent, 2020).
3. L. Engelke, G. Winter, S. Hook, and J. Engert, "Recent Insights into Cutaneous Immunization: How to Vaccinate via the Skin," *Vaccine* 33 (2015): 4663–4674.
4. L.-y Long, J. Zhang, Z. Yang, Y. Guo, X. Hu, and Y. Wang, "Transdermal Delivery of Peptide and Protein Drugs: Strategies, Advantages and Disadvantages," *Journal of Drug Delivery Science and Technology* 60 (2020): 102007.
5. W. Y. Jeong, M. Kwon, H. E. Choi, and K. S. Kim, "Recent Advances in Transdermal Drug Delivery Systems: A Review," *Biomaterials Research* 25 (2021): 24.
6. M. R. Prausnitz and R. Langer, "Transdermal Drug Delivery," *Nature Biotechnology* 26 (2008): 1261–1268.
7. M. S. Gerstel and V. A. Place, "Drug Delivery Device," *US-3964482-A* (United States Patent, 1976).
8. T. Waghule, G. Singhvi, S. K. Dubey, et al., "A Smart Approach and Increasing Potential for Transdermal Drug Delivery System," *Biomedicine & Pharmacotherapy* 109 (2019): 1249–1258.
9. J. Yang, X. Liu, Y. Fu, and Y. Song, "Recent Advances of Microneedles for Biomedical Applications: Drug Delivery and beyond," *Acta Pharmaceutica Sinica B*, 9 (2019): 469–483.
10. K. M. Saifullah and R. Z. Faraji, "Sampling Dermal Interstitial Fluid Using Microneedles: a Review of Recent Developments in Sampling Methods and Microneedle-based Biosensors," *Advanced Materials Interfaces* 10 (2023): 2201763.
11. K. M. Kwon, S. M. Lim, S. Choi, et al., "Microneedles: Quick and Easy Delivery Methods of Vaccines," *Clinical and Experimental Vaccine Research* 6 (2017): 156–159.
12. K. T. Chang, Y. K. Shen, F. Y. Fan, Y. Lin, and S. C. Kang, "Optimal Design and Fabrication of a Microneedle Arrays Patch," *Journal of Manufacturing Processes* 54 (2020): 274–285.
13. Y. Ghiyasi, P. D. Prewett, G. J. Davies, and Z. Faraji Rad, "The Role of Microneedles in the Healing of Chronic Wounds," *International Journal of Pharmaceutics* 641 (2023): 123087.
14. M. R. Prausnitz, "Engineering Microneedle Patches for Vaccination and Drug Delivery to Skin," *Annual Review of Chemical and Biomolecular Engineering* 8 (2017): 177–200.
15. E. Z. Loizidou, N. T. Inoue, J. Ashton-Barnett, D. A. Barrow, and C. J. Allender, "Evaluation of Geometrical Effects of Microneedles on Skin Penetration by CT Scan and Finite Element Analysis," *European Journal of Pharmaceutics and Biopharmaceutics* 107 (2016): 1–6.
16. N. Akhtar, "Microneedles: an Innovative Approach to Transdermal Delivery-a Review," *International Journal of Pharmacy and Pharmaceutical Sciences* 6 (2014): 18–25.
17. A. H. Sabri, Y. Kim, M. Marlow, et al., "Intradermal and Transdermal Drug Delivery Using microneedles—Fabrication, Performance Evaluation and Application to Lymphatic Delivery," *Advanced Drug Delivery Reviews* 153 (2020): 195–215.

18. R. Nagarkar, M. Singh, H. X. Nguyen, and S. Jonnalagadda, "A Review of Recent Advances in Microneedle Technology for Transdermal Drug Delivery," *Journal of Drug Delivery Science and Technology* 59 (2020): 101923.
19. Z. Faraji Rad, P. D. Prewett, and G. J. Davies, "An Overview of Microneedle Applications, Materials, and Fabrication Methods," *Beilstein Journal of Nanotechnology* 12 (2021): 1034–1046.
20. E. Larrañeta, R. E. Lutton, A. D. Woolfson, and R. F. Donnelly, "Microneedle Arrays as Transdermal and Intradermal Drug Delivery Systems: Materials Science, Manufacture and Commercial Development," *Materials Science and Engineering: R: Reports* 104 (2016): 1–32.
21. X. Luo, L. Yang, and Y. Cui, "Microneedles: Materials, Fabrication, and Biomedical Applications," *Biomedical Microdevices* 25 (2023): 20.
22. K. Ita, "Ceramic Microneedles and Hollow Microneedles for Transdermal Drug Delivery: Two Decades of Research," *Journal of Drug Delivery Science and Technology* 44 (2018): 314–322.
23. M. Azmana, S. Mahmood, A. R. Hilles, U. K. Mandal, A. I. J. KAS, and S. Raman, "Transdermal Drug Delivery System through Polymeric Microneedle: a Recent Update," *Journal of Drug Delivery Science and Technology* 60 (2020): 101877.
24. J. W. Lee, M. R. Han, and J. H. Park, "Polymer Microneedles for Transdermal Drug Delivery," *Journal of Drug Targeting* 21 (2013): 211–223.
25. S. Mdanda, P. Ubanako, P. P. Kondiah, P. Kumar, and Y. E. Choonara, "Recent Advances in Microneedle Platforms for Transdermal Drug Delivery Technologies," *Polymers* 13 (2021): 2405.
26. X. Hong, L. Wei, F. Wu, et al., "Dissolving and Biodegradable Microneedle Technologies for Transdermal Sustained Delivery of Drug and Vaccine," *Drug Design, Development and Therapy* 7 (2013): 945–952.
27. E. M. Cahill and E. D. O'Cearbhaill, "Toward Biofunctional Microneedles for Stimulus Responsive Drug Delivery," *Bioconjugate Chemistry* 26 (2015): 1289–1296.
28. R. X. Liu, Y. T. He, L. Liang, et al., "Mechanical Evaluation of Polymer Microneedles for Transdermal Drug Delivery: In Vitro and in Vivo," *Journal of Industrial and Engineering Chemistry* 114 (2022): 181–189.
29. G. Bonfante, H. Lee, L. Bao, J. Park, N. Takama, and B. Kim, "Comparison of Polymers to Enhance Mechanical Properties of Microneedles for Bio-medical Applications," *Micro and Nano Systems Letters* 8 (2020): 1–13.
30. J. H. Park and M. R. Prausnitz, "Analysis of Mechanical Failure of Polymer Microneedles by Axial Force," *The Journal of the Korean Physical Society* 56 (2010): 1223.
31. M. Gülçür, E. Brown, T. Gough, and B. Whiteside, "Characterisation of Microneedle Replication and Flow Behaviour in Ultrasonic Micro-injection Moulding through Design of Experiments," *Journal of Manufacturing Processes* 102 (2023): 513–527.
32. T. E. Andersen, A. J. Andersen, R. S. Petersen, L. H. Nielsen, and S. S. Keller, "Drug Loaded Biodegradable Polymer Microneedles Fabricated by Hot Embossing," *Microelectronic Engineering* 195 (2018): 57–61.
33. S. Yang, Y. Feng, L. Zhang, N. Chen, W. Yuan, and T. Jin, "A Scalable Fabrication Process of Polymer Microneedles," *International Journal of Nanomedicine* 7 (2012): 1415–1422.
34. M. A. Luzuriaga, D. R. Berry, J. C. Reagan, R. A. Smaldone, and J. J. Gassensmith, "Biodegradable 3D Printed Polymer Microneedles for Transdermal Drug Delivery," *Lab on a Chip* 18 (2018): 1223–1230.
35. L. Wu, J. Park, Y. Kamaki, and B. Kim, "Optimization of the Fused Deposition Modeling-based Fabrication Process for Polylactic Acid Microneedles," *Microsystems & Nanoengineering* 7 (2021): 58.
36. Z. Faraji Rad, P. D. Prewett and G. J. Davies, "High-resolution Two-photon Polymerization: the Most Versatile Technique for the Fabrication of Microneedle Arrays," *Microsystems & Nanoengineering*, 7 (2021): 71.
37. K. Lee, H. C. Lee, D. S. Lee, and H. Jung, "Drawing Lithography: Three-dimensional Fabrication of an Ultrahigh-aspect-ratio Microneedle," *Advanced Materials* 22 (2010): 483–486.
38. M. Gülçür, J. M. Romano, P. Penchev, et al., "A Cost-effective Process Chain for Thermoplastic Microneedle Manufacture Combining Laser Micro-machining and Micro-injection Moulding," *CIRP Journal of Manufacturing Science and Technology* 32 (2021): 311–321.
39. J. W. Jor, M. D. Parker, A. J. Taberner, M. P. Nash, and P. M. Nielsen, "Computational and Experimental Characterization of Skin Mechanics: Identifying Current Challenges and Future Directions," *Wiley Interdisciplinary Reviews: Systems Biology and Medicine* 5 (2013): 539–556.
40. M. Shikida, S. Kitamura, C. Miyake, and K. Bessho, "Micromachined Pyramidal Shaped Biodegradable Microneedle and Its Skin Penetration Capability," *Microsystem technologies* 20 (2014): 2239–2245.
41. P. G. Agache, P. Agache, and P. Humbert, *Measuring the Skin* (Springer Science & Business Media, 2004).
42. X. Liu, J. Cleary, and G. German, "The Global Mechanical Properties and Multi-scale Failure Mechanics of Heterogeneous human Stratum Corneum," *Acta Biomaterialia* 43 (2016): 78–87.
43. P. M. Elias, "The Stratum Corneum as an Organ of Protection: Old and New Concepts," *Immunodeficiency and Skin* 18 (1989): 10–21.
44. V. Ebrahiminejad, P. D. Prewett, Z. Faraji Rad and G. J. Davies, "Microneedle Arrays for Drug Delivery and Diagnostics: toward an Optimized Design, Reliable Insertion, and Penetration," *Advanced Materials Interfaces* 9 (2022): 2101856.
45. R. F. Donnelly, M. J. Garland, D. I. Morrow, et al., "Optical Coherence Tomography Is a Valuable Tool in the Study of the Effects of Microneedle Geometry on Skin Penetration Characteristics and in-skin Dissolution," *Journal of Controlled Release* 147 (2010): 333–341.
46. R. F. Donnelly, T. R. R. Singh, E. Larrañeta, and M. T. McCrudden, *Microneedles for Drug and Vaccine Delivery and Patient Monitoring* (John Wiley & Sons, 2018).
47. M. C. Chen, S. F. Huang, K. Y. Lai, and M. H. Ling, "Fully Embeddable chitosan microneedles as a Sustained Release Depot for Intradermal Vaccination," *Biomaterials* 34 (2013): 3077–3086.
48. K. M. Saifullah, P. Azarikhah, and Z. Faraji Rad, "Synthesis-free Swellable Hydrogel Microneedles for Rapid Interstitial Fluid Extraction and on-site Glucose Detection via an Electrochemical Biosensor System," *Materials Today Chemistry* 45 (2025): 102661.
49. G. Ma and C. Wu, "bio-microneedle and bio-inspired microneedle: a Review," *Journal of Controlled Release* 251 (2017): 11–23.
50. S. A. Ranamukhaarachchi and B. Stoeber, "Determining the Factors Affecting Dynamic Insertion of Microneedles into Skin," *Biomedical Microdevices* 21 (2019): 1–8.
51. V. Ebrahiminejad, Z. Faraji Rad and A. Malek-khatibi, "Influence of Low-Frequency Vibration and Skin Strain on Insertion Mechanics and Drug Diffusion of PVA/PVP Dissolving Microneedles," *Advanced Materials Technologies* 9 (2024): 2301272.
52. O. Olatunji, D. B. Das, M. J. Garland, L. Belaid, R. F. Donnelly, "Influence of Array Interspacing on the Force Required for Successful Microneedle Skin Penetration: Theoretical and Practical Approaches," *Journal of Pharmaceutical Sciences* 102 (2013): 1209–1221.
53. K. M. Saifullah, A. Mushtaq, P. Azarikhah, P. D. Prewett, Z. Faraji Rad and G. J. Davies, "Micro-vibration Assisted Dual-layer Spiral Microneedles to Rapidly Extract Dermal Interstitial Fluid for Minimally Invasive Detection of Glucose," *Microsystems & Nanoengineering* 11 (2025): 3.
54. Y. Ma, X. Xiao, H. Ren, and M. Q.-H. Meng, "A Review of Bio-inspired Needle for Percutaneous Interventions," *Biomimetic Intelligence and Robotics* 2 (2022): 100064.
55. Q. Yan, J. Weng, S. Shen, et al., "Finite Element Analysis for Biodegradable Dissolving Microneedle Materials on Skin Puncture and Mechanical Performance Evaluation," *Polymers* 13 (2021): 3043.
56. F. Henriquez, J. O. Morales-Ferreiro, and D. Celentano, "Structural Evaluation by the Finite-Element Method of Hollow Microneedle Geome-

- tries for Drug Delivery," *Advanced Engineering Materials* 24 (2022): 2200049.
57. L. Zhang, C. Zhu, J. Shi, Z. Zhou, and D. Ge, "Design of Three-section Microneedle towards Low Insertion Force and High Drug Delivery Amount Using the Finite Element Method," *Computer Methods in Biomechanics and Biomedical Engineering* 27 (2024): 156–166.
58. S. Chandbadshah and G. Mannayee, "Structural Analysis and Simulation of Solid Microneedle Array for Vaccine Delivery Applications," *Materials Today: Proceedings* 65 (2022): 3774–3779.
59. T. Liu, Y. Sun, W. Zhang, et al., "Mechanical Investigation of Solid MNs Penetration into Skin Using Finite Element Analysis," *Advanced Engineering Materials* 26 (2024): 2301532.
60. W. Wang, Y. Liang, X. Yan, G. Tang, F. Xu, and Z. Li, "Based on Finite Element Simulation: Optimization of Microneedle Structure and Mechanical Performance Analysis," in *2024 International Conference on Applied Mathematics, Modelling and Statistics Application* (IOP Publishing, 2024).
61. X. Zhang, Q. Gu, X. Sui, J. Zhang, J. Liu, and R. Zhou, "Design and Optimization of Hollow Microneedle Spacing for Three Materials Using Finite Element Methods," *Scientific Reports* 15 (2025): 652.
62. W. Shu, H. Heimark, N. Bertollo, D. J. Tobin, E. D. O'Cearbhaill, and A. N. Annaidh, "Insights into the Mechanics of Solid Conical Microneedle Array Insertion into Skin Using the Finite Element Method," *Acta Biomaterialia* 135 (2021): 403–413.
63. X. Kong, P. Zhou, and C. Wu, "Numerical Simulation of Microneedles' insertion into Skin," *Computer Methods in Biomechanics and Biomedical Engineering* 14 (2011): 827–835.
64. S. P. Davis, B. J. Landis, Z. H. Adams, M. G. Allen, and M. R. Prausnitz, "Insertion of Microneedles into Skin: Measurement and Prediction of Insertion Force and Needle Fracture Force," *Journal of Biomechanics* 37 (2004): 1155–1163.
65. I. Xenikakis, M. Tzimtzimis, K. Tsongas, et al., "Fabrication and Finite Element Analysis of Stereolithographic 3D Printed Microneedles for Transdermal Delivery of Model Dyes across human Skin in Vitro," *European Journal of Pharmaceutical Sciences* 137 (2019): 104976.
66. H. Takehara, M. Inada, Y. Kanda, and T. Ichiki, "Mechanical Finite Element Analysis of Needle Tip Shape to Develop Insertable Polymer-based Microneedle without Plastic Deformation," *Journal of the Mechanical Behavior of Biomedical Materials* 163 (2025): 106885.
67. C. Radhika and B. Gnanavel, "Finite Element Analysis of Polymer Microneedle for Transdermal Drug Delivery," *Materials Today: Proceedings* 39 (2021): 1538–1542.
68. E. Z. Loizidou, N. A. Williams, D. A. Barrow, et al., "Structural Characterisation and Transdermal Delivery Studies on Sugar Microneedles: Experimental and Finite Element Modelling Analyses," *European Journal of Pharmaceutics and Biopharmaceutics* 89 (2015): 224–231.
69. U. Kanakaraj and T. Lhaden, "Analysis of Structural Mechanics of Solid Microneedle Using COMSOL Software," in *2015 International Conference on Innovations in Information, Embedded and Communication Systems (Iciiecs)* (IEEE, 2015).
70. A. Römgen, D. Bader, J. Bouwstra, F. Baaijens, and C. Oomens, "Monitoring the Penetration Process of Single Microneedles with Varying Tip Diameters," *Journal of the Mechanical Behavior of Biomedical Materials* 40 (2014): 397–405.
71. P. R. Yadav, T. Han, O. Olatunji, S. K. Pattanayek, and D. B. Das, "Mathematical Modelling, Simulation and Optimisation of Microneedles for Transdermal Drug Delivery: Trends and Progress," *Pharmaceutics* 12 (2020): 693.
72. B. Ahn, "Optimal Microneedle Design for Drug Delivery Based on Insertion Force Experiments with Variable Geometry," *International Journal of Control, Automation and Systems* 18 (2020): 143–149.
73. V. Ebrahiminejad, Z. Faraji Rad "Design, Development, and Testing of Polymeric Microblades: a Novel Design of Microneedles for Biomedical Applications," *Advanced Materials Interfaces* 9 (2022): 2201115.
74. K. Biniek, J. Kaczvinsky, P. Matts, and R. H. Dauskardt, "Understanding Age-induced Alterations to the Biomechanical Barrier Function of human Stratum Corneum," *Journal of Dermatological Science* 80 (2015): 94–101.
75. T. Tsugita, T. Nishijima, T. Kitahara, and Y. Takema, "Positional Differences and Aging Changes in Japanese Woman Epidermal Thickness and Corneous Thickness Determined by OCT (optical coherence tomography)," *Skin Research and Technology* 19 (2013): 242–250.
76. I. Dulińska-Molak, M. Pasikowska, K. Pogoda, M. Lewandowska, I. Eris, and M. Lekka, "Age-related Changes in the Mechanical Properties of human Fibroblasts and Its Prospective Reversal after Anti-wrinkle Tripeptide Treatment," *International Journal of Peptide Research and Therapeutics* 20 (2014): 77–85.
77. Y. Hara, Y. Masuda, T. Hirao, and N. Yoshikawa, "The Relationship between the Young's Modulus of the Stratum Corneum and Age: a Pilot Study," *Skin Research and Technology* 19 (2013): 339–345.
78. F. Zhu, "Modeling of Blast Wave and Its Effect on the Human/Animal Body," *Basic Finite Element Method as Applied to Injury Biomechanics* (Elsevier, 2018).
79. V. Ebrahiminejad, Z. Faraji Rad, P. D. Prewett, and G. J. Davies, "Fabrication and Testing of Polymer Microneedles for Transdermal Drug Delivery," *Beilstein Journal of Nanotechnology* 13 (2022): 629–640.
80. Z. Faraji Rad, R. E. Nordon, C. J. Anthony, and L. Bilston, et al., "High-fidelity Replication of Thermoplastic Microneedles with Open Microfluidic Channels," *Microsystems & Nanoengineering* 3 (2017): 1–11.
81. Liquid Crystal Polymer Medical Grade, accessed October 9, 2024, <https://www.celanese.com/products/medical-vecra-lcp-mt-zenite>.
82. R. D. Boehm, J. Daniels, S. Stafslie, A. Nasir, J. Lefebvre, and R. J. Narayan, "Polyglycolic Acid Microneedles Modified with Inkjet-deposited Antifungal Coatings," *Biointerphases* 10 (2015).
83. K. Assani, A. Neidhard-Doll, and T. Goswami, "Mechanical Properties of Nanoparticles in the Drug Delivery Kinetics," *Journal of Pharmaceutical and Biopharmaceutical Research* (2022): 248–255.
84. S. Rahrovan, F. Fanian, P. Mehryan, P. Humbert, and A. Firooz, "Male versus Female Skin: What Dermatologists and Cosmeticians Should Know," *International Journal of Women's Dermatology* 4 (2018): 122–130.
85. M. A. Serrat, C. J. Vinyard, and D. King, "Alterations in the Mechanical Properties and Composition of Skin in human Growth Hormone Transgenic Mice," *Connective Tissue Research* 48 (2007): 19–26.
86. S. Luebberding, N. Krueger, and M. Kerscher, "Mechanical Properties of human Skin in Vivo: a Comparative Evaluation in 300 Men and Women," *Skin Research and Technology* 20 (2014): 127–135.
87. S. Diridollou, D. Black, J. Lagarde, et al., "Sex-and Site-dependent Variations in the Thickness and Mechanical Properties of human Skin in Vivo," *International Journal of Cosmetic Science* 22 (2000): 421–435.
88. O. A. Shergold, N. A. Fleck, and D. Radford, "The Uniaxial Stress versus Strain Response of Pig Skin and Silicone Rubber at Low and High Strain Rates," *International Journal of Impact Engineering* 32 (2006): 1384–1402.
89. H. Alexander and T. Cook, "Variations with Age in the Mechanical Properties of human Skin in Vivo," *Journal of Tissue Viability* 16 (2006): 6–11.
90. A. M. Kligman, "Early Destructive Effect of Sunlight on human Skin," *Jama* 210 (1969): 2377–2380.
91. M. El-Domyati, S. Attia, F. Saleh, et al., "Intrinsic Aging vs. photoaging: a Comparative Histopathological, Immunohistochemical, and Ultrastructural Study of Skin," *Experimental Dermatology* 11 (2002): 398–405.

92. A. M. Okamura, C. Simone, and M. D. O'leary, "Force Modeling for Needle Insertion into Soft Tissue," *IEEE Transactions on Biomedical Engineering* 51 (2004): 1707–1716.
93. J. T. Hing, A. D. Brooks, and J. P. Desai, "Reality-based Needle Insertion Simulation for Haptic Feedback in Prostate Brachytherapy," in *Proceedings 2006 IEEE International Conference on Robotics and Automation*, (IEEE, 2006).
94. S. Jiang, P. Li, Y. Yu, J. Liu, and Z. Yang, "Experimental Study of Needle–tissue Interaction Forces: Effect of Needle Geometries, Insertion Methods and Tissue Characteristics," *Journal of biomechanics* 47 (2014): 3344–3353.
95. M. Mahvash and P. E. Dupont, "Mechanics of Dynamic Needle Insertion into a Biological Material," *IEEE transactions on biomedical engineering* 57 (2009): 934–943.
96. J. Ling, L. Jiang, K. Chen, et al., "Insertion and Pull Behavior of Worker honeybee stinger," *Journal of Bionic Engineering* 13 (2016): 303–311.
97. S. Davis, M. Prausnitz, and M. Allen. "Fabrication and Characterization of Laser Micromachined Hollow Microneedles. in TRANSDUCERS'03," 12th International Conference on Solid-State Sensors, Actuators and Microsystems. Digest of Technical Papers (IEEE, 2003)..
98. J. H. Park, Y. K. Yoon, S. O. Choi, M. R. Prausnitz, and M. G. Allen, "Tapered Conical Polymer Microneedles Fabricated Using an Integrated Lens Technique for Transdermal Drug Delivery," *IEEE Transactions on Biomedical Engineering* 54 (2007): 903–913.
99. J. Ling, Z. Song, J. Wang, et al., "Effect of Honeybee Stinger and Its Microstructured Barbs on Insertion and Pull Force," *Journal of the Mechanical Behavior of Biomedical Materials* 68 (2017): 173–179.
100. X. Zhang, C. Zhou, T. Chen, et al., "State-of-the-art Strategies to Enhance the Mechanical Properties of Microneedles," *International Journal of Pharmaceutics* 63 (2024): 124547.

Supporting Information

Additional supporting information can be found online in the Supporting Information section.

Supporting File 1: mame70057-sup-0001-SuppMat.docx. **Supporting**

File 2: mame70057-sup-0002-Videos.pptx.